

Crazing Mechanism and Physical Aging of Poly(lactide) Toughened with Poly(ethylene oxide)-*block*-poly(butylene oxide) Diblock Copolymers

Charles J. McCutcheon,[†] Boran Zhao,[†] Kailong Jin, Frank S. Bates,^{*} and Christopher J. Ellison^{*}

Cite This: *Macromolecules* 2020, 53, 10163–10178

Read Online

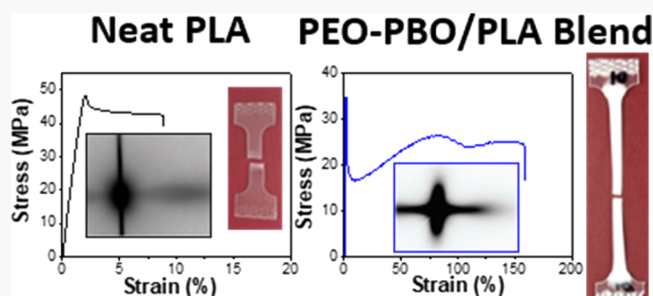
ACCESS |

Metrics & More

Article Recommendations

Supporting Information

ABSTRACT: Sustainable polymers are important alternatives to plastics and elastomers derived from petroleum resources. Poly(lactide) (PLA), a commercially available sustainable plastic, is a well-known success story. However, PLA lacks ductility and toughness, limiting the number of potential uses. In this study, small amounts of a liquid poly(ethylene oxide)-*block*-poly(butylene oxide) (PEO-PBO) diblock copolymer additive were blended with PLA to enhance its toughness and ductility. The incorporated PEO-PBO diblock copolymers generated a macrophase-separated morphology with particle diameters of 0.2–0.9 μm , and nearly matched refractive indices of PLA and PEO-PBO led to retention of optical transparency. Addition of just 1.8 wt % PEO-PBO into PLA led to a 20-fold increase in toughness, measured as the area under the stress–strain data in tension without affecting the bulk elastic modulus of the plastic. The micromechanical deformation process of the PEO-PBO/PLA blend was investigated via in situ small angle X-ray scattering during tensile testing. The total volume of the crazed material was proportional to the total surface area of the dispersed PEO-PBO particles, and both quantities increased with increasing PEO-PBO loading. Increasing the PEO-PBO loading also resulted in (A) an increase in particle size, causing a decrease in the craze initiation stress, and (B) an increase in fibril spacing, indicating a lower craze propagation stress. Furthermore, craze development was found to be independent of aging time. As a result, the PEO-PBO/PLA blend was able to remain ductile and tough for up to 114 days, exhibiting a 10-fold increase in elongation at break and toughness compared to neat PLA, which becomes brittle in less than 2 days. These results demonstrate that designing additives that promote deformation by crazing is an effective way to overcome the aging-induced embrittlement of glassy polymers.



1. INTRODUCTION

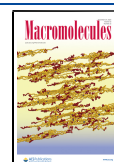
Sustainability is a key aspect for greener global economic growth. Therefore, addressing plastic pollution, including identifying viable alternatives for petroleum-based plastics (e.g., polyethylene, polystyrene, and polyethylene terephthalate), is increasingly urgent.^{1,2} Poly(lactide) (PLA) is a commercially available sustainable polymer that is both bio-sourced and compostable.^{3,4} PLA has an annual global production of 190,000 tons (in 2019)⁵ with applications ranging from disposable utensils to plastic packaging to 3D printing filaments.⁶ In industry, PLA is usually melt-processed above its glass transition temperature ($T_g = 55\text{--}60\text{ }^\circ\text{C}$) and then rapidly quenched below its T_g , ultimately to room temperature. The rapid quench produces a non-equilibrium glassy state with excess free volume that facilitates relaxation toward equilibrium through a densification process called physical aging. PLA is one of many glassy polymers that is known to undergo physical aging, which consequently leads to mechanical embrittlement over a short period of time (ca. less than 2 days),^{7–12} limiting its viability in many applications.

Several routes have been reported for toughening PLA. One method is the addition of miscible, low-molar-mass plasticizers such as poly(ethylene oxide) (PEO),^{13–15} triacetin,¹⁶ and citrate esters,¹⁷ which also decreases the T_g . To properly toughen PLA, a relatively high plasticizer loading (>10 wt %) is often required, which inevitably leads to several undesirable characteristics, e.g., concerns of leaching, decreased upper service and heat distortion temperatures, and reduced modulus.¹⁸ An alternative and economical way to toughen PLA is through addition of rubbery particle inclusions, i.e., blending PLA with immiscible rubbery polymeric additives including poly(caprolactone),^{19,20} linear low-density polyethylene,^{21,22} poly(dimethylsiloxane),²³ and acrylonitrile–butadiene–styrene copolymers.²⁴ Due to their relatively low

Received: July 29, 2020

Revised: October 5, 2020

Published: November 3, 2020



moduli compared with the PLA matrix, the rubbery particles can act as stress concentrators that promote plastic deformation in the surrounding matrix.^{25,26} The effect of particle size on PLA toughening performance has been carefully examined in previous studies, which has led to a conclusion that an ideal particle size range, i.e., 0.7–1.1 μm , maximizes the toughness in the PLA blends.^{4,27–29} When the rubbery particles are too large, they can cavitate and adversely act as catastrophic voids that initiate cracks. In contrast, when the rubbery particles are too small, they can neither cavitate nor act as effective stress concentrators. Although high shear mixing during melt processing and use of a compatibilizer (i.e., in addition to the PLA matrix and rubbery additive, making a ternary blend) are often applied to obtain properly sized rubbery particles, it is challenging to stabilize the dispersed phase due to coalescence of the rubbery particles over time.⁴

A more attractive solution to precisely control and stabilize the rubber particle size is the use of amphiphilic diblock copolymer additives. Diblock copolymers consist of two homopolymer chains linked by a single covalent bond.³⁰ When composed of a matrix-philic block and a matrix-phobic, rubbery block, they can form dispersions in the PLA matrix that combine the functions of a compatibilizer and rubbery particles, producing dispersed particles with precisely controlled sizes using a single additive.³⁰ Poly(ethylene oxide) (PEO) has been commonly used as a matrix-philic block due to its favorable interactions with PLA,^{31–35} while poly(butylene oxide) (PBO) and poly(propylene oxide) (PPO) have served as the matrix-phobic block for their rubbery nature as both have a $T_g \approx -70^\circ\text{C}$. Previous studies have shown that such PEO-based block copolymers can function as effective toughening agents for PLA.^{36–38} For example, Li et al.³⁹ and Gu et al.⁴⁰ blended PEO-PBO and PEO-PPO-PEO (a symmetric triblock polymer) into PLA, leading to 13- and 11-fold improvements in toughness compared to neat PLA, respectively. Although previous studies of PLA/block copolymer blends have shown promising toughening results, several fundamental aspects have yet to be clearly addressed; for example, the details of the underlying toughening mechanism and nature of the micro-deformation events (e.g., crazing, shear yielding, and particle cavitation) are still unclear. Another underexplored aspect is how physical aging affects the toughness and the toughening mechanism over time. Improvement in toughness induced by inclusion of rubber particles has rarely been studied as a function of aging time. Understanding these fundamental aspects will further enable the development of more effective toughening methods for PLA and other polymers that undergo physical aging-induced embrittlement.

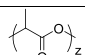
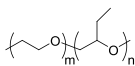
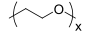
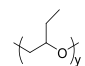
Herein, we report a facile route to produce tough amorphous PLA materials by blending commercially available PEO-PBO diblock copolymers in a PLA matrix. Notably, the resulting liquid dispersions in the PLA matrix do not sacrifice the sample transparency because the components possess matched refractive indices. First, we demonstrated the advantage of the diblock molecular architecture by comparing the morphological and tensile properties of the PEO-PBO/PLA blends with those of corresponding homopolymer/PLA blends (i.e., PEO/PLA and PBO/PLA). Second, the effect of the PEO-PBO concentration on blend toughness was examined and the micromechanical deformation process of the PEO-PBO/PLA blend was systematically investigated via in situ small angle X-ray scattering (SAXS) during tensile testing. Classical models of particle cavitation and craze

formation were applied to understand the underlying toughening mechanism. Finally, the impact of physical aging on the toughness of PEO-PBO/PLA blends was evaluated, and the long-term toughening performance and the associated toughening mechanism were revealed.

2. EXPERIMENTAL SECTION

2.1. Materials. Amorphous-grade PLA (PLA4060D) was purchased from NatureWorks. The diblock copolymer (PEO-PBO), under the trade name Fortegra 100, was purchased from Olin Corporation. A PEO homopolymer was purchased from Sigma Aldrich. A PBO homopolymer was synthesized by anionic polymerization as described previously.⁴¹ The chemical structures and molecular characteristics of PLA, PEO, PBO, and PEO-PBO are displayed in Table 1. Detailed procedures of polymer synthesis and characterization are provided in the Supporting Information.

Table 1. Chemical Structures and Molecular Characteristics of Polymers Used in This Study

Polymer	Polymer Structure	M_n (kg/mol)	PEO Volume Fraction ^d	Dispersity ^e
PLA		83 ^a	--	1.53
PEO-PBO		7.4 ^b	0.35	1.04
PEO		5.0 ^c	1	1.02
PBO		6.9 ^c	--	1.17

^a M_n was measured by size exclusion chromatography–multiangle light scattering (SEC-MALS) with a tetrahydrofuran (THF) mobile phase and $dn/dc = 0.047$ calculated assuming 100% sample recovery.

^b M_n was measured by laser-assisted MALDI. ^c M_n was measured by end group analysis with ¹H NMR. ^dPEO volume fraction was calculated from ¹H NMR assuming $\rho_{\text{PEO}} = 1.07$ and $\rho_{\text{PBO}} = 0.92$ according to ref 42. ^eDispersity was measured by SEC-MALS with a THF mobile phase.

2.2. Sample Preparation. **2.2.1. PEO-PBO/PLA Blend.** Pellets of the PEO-PBO/PLA blend with varying composition were prepared using a masterbatch-dilution method. The PLA pellets and the diblock copolymer were vacuum-dried at 50 $^\circ\text{C}$ for 24 h before melt mixing. A concentrated PEO-PBO/PLA blend (called the masterbatch) was first prepared by melt blending using a 16 mm twin-screw extruder (PRISM, L:D = 24:1) operating at 60 rpm with zone temperatures set to 120, 140, 160, and 180 $^\circ\text{C}$ from the hopper to die. After a steady flow rate (20 g/min) of neat PLA was established, the viscous PEO-PBO liquid was added to the hopper at a rate of 2 g/min using a syringe pump. The extrudate was water-chilled, machine-pelletized, and vacuum-dried at 50 $^\circ\text{C}$ for 48 h. The concentration of PEO-PBO in the masterbatch was confirmed to be 10 wt % by ¹H NMR analysis (see Figure S1 in the Supporting Information for detailed analysis). The masterbatch pellets were then physically mixed with a predetermined amount of neat PLA pellets and subsequently melt-extruded following the same processing parameters as the masterbatch. A series of PEO-PBO/PLA blend pellets with PEO-PBO loadings of 0.8, 1.8, 3.0, 4.7, and 6.0 wt % were achieved, where the composition was quantified by ¹H NMR. It was confirmed through size exclusion chromatography (SEC) analysis that the blending procedure does not degrade PLA (Figure S2 in the Supporting Information).

2.2.2. PBO/PLA and PEO/PLA Blends. Due to small available quantities of the synthesized PBO and purchased PEO homopolymers, PBO/PLA and PEO/PLA blends were prepared using a

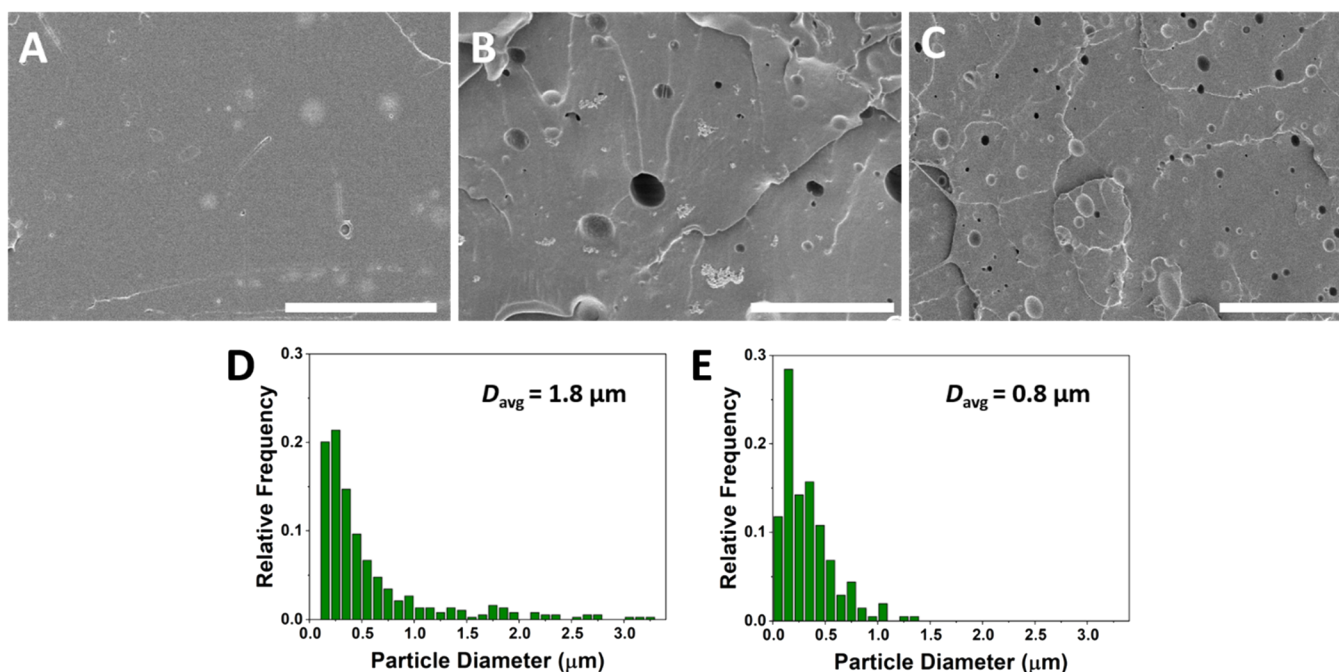


Figure 1. Morphologies of PLA blends with (A) 5 wt % PEO, (B) 4.6 wt % PBO, and (C) 4.7 wt % PEO-PBO after being compression-molded into films, fractured, and rinsed with methanol. Corresponding particle diameter distributions with (D) 4.6 wt % PBO and (E) 4.7 wt % PEO-PBO/PLA. The scale bars represent 10 μm .

microcompounder (Xplore) with a 5 mL empty chamber volume. The liquid PBO was solidified using liquid nitrogen so that it could be placed in the hopper and pushed into the barrel by a predetermined amount of PLA pellets. The mixture was melt-blended for 5 min at 180 °C and 100 rpm, extruded, and chilled by liquid nitrogen. The weight fraction of PBO in PLA was determined by ^1H NMR.

2.3. Characterization. **2.3.1. Tensile Testing.** To evaluate the effect of the different additives (PEO, PBO, and PEO-PBO) on the mechanical properties of the resulting PLA blends, uniaxial tensile tests were performed. The pellets of PLA blends and neat PLA were compression-molded (Carver hydraulic press) into $\sim 300 \mu\text{m}$ -thick films at 135 °C for 5 min and then quenched to room temperature within 1 min. After forming the films, standard dumbbell-shaped tensile bars were prepared according to ASTM D1708 using a dumbbell cutter (Dumbbell Co., Ltd. SDL200, equipped with an SDMK-1000 dumbbell cutter). The tensile tests were performed at room temperature using a tensile tester (Instron 5966) operated at 1 mm/min according to ASTM D1708. The tensile properties, including Young's modulus (E), yield stress (σ_y), and elongation at break (ϵ_B), were averaged from at least six separate test specimens.

2.3.2. Scanning Electron Microscopy (SEM) and Particle Size Analysis. Blend morphologies were characterized by SEM (Hitachi S-4700). Both the pellets and the corresponding films were cryo-fractured in liquid nitrogen. The fractured surface was rinsed with methanol for 1 min at room temperature to dissolve the dispersed phase, vacuum-dried for 2 h at 50 °C, and sputter-coated with 5 nm iridium before SEM characterization. SEM images were processed by ImageJ to characterize the dispersed phase particle size and particle size distribution following procedures described elsewhere.⁴³ The particle diameter was calculated by an area weighted average, and the ratio of area weighted average/number averaged diameter was taken as the polydispersity.⁴³ The reported “ \pm ” is one standard deviation about the mean, and at least three SEM images (about 1000 particles in total) were processed for each sample. Detailed analyses of the particle sizes are provided in the [Supporting Information](#).

2.3.3. Transmission Electron Microscopy (TEM). Samples were prepared from the gauge region of elongated tensile bars to analyze the sample deformation. Ultrathin 70 nm sections were cut along the sample strain direction (to distinguish between knife marks and deformation features) with a diamond knife (Diatome) by cryo-

microtoming at $-120 \text{ }^\circ\text{C}$ on an ultramicrotome (Leica EM UC6 with FC-S Cryo attachment). Sections were vapor-stained with 0.5 wt % ruthenium tetroxide (RuO_4) in water. All samples were imaged on a TEM (Tecnai G2 Spirit Biotwin) at an operating voltage of 120 kV.

2.3.4. Differential Scanning Calorimetry (DSC). DSC analysis was performed on melt-processed neat PLA and PLA-additive blends using a Mettler Toledo DSC 1. Approximately 5 mg of sample was loaded into a hermetically sealed aluminum pan with a pinhole on the top. Samples were heated to 135 °C at 10 °C/min and held isothermally for 5 min to eliminate the effect of thermal history and then cooled to $-100 \text{ }^\circ\text{C}$ at $-10 \text{ }^\circ\text{C}/\text{min}$ and held isothermally for 5 min. Samples were then re-heated to 135 °C at 10 °C/min (i.e., a typical second heating step), from which the T_g was determined. All DSC experiments were performed under an inert nitrogen atmosphere.

2.3.5. Small-Angle X-ray Scattering (SAXS). Synchrotron SAXS data were acquired from the DND-CAT SID-D beamline at the Advanced Photon Source (Argonne, IL). The data were collected using a sample-to-detector distance of 8.5 m and a photon wavelength of $\lambda = 1.3776 \text{ \AA}$. Two-dimensional (2D) scattering patterns were recorded using a Rayonix CCD detector. The tensile bars for all SAXS measurements were elongated in the vertical direction identified as 90°. The 2D SAXS patterns were then integrated (1) radially, producing a 1D plot of intensity vs azimuth angle, and (2) over azimuthal angles from -10° to 10° (i.e., perpendicular to the strain direction of 90°), generating a plot of intensity vs scattering vector $q = 4\pi\lambda^{-1}\sin(\theta/2)$ vs intensity. The intensity displayed in the 1D plots is presented as “Intensity (normalized)”, where the measured intensity was divided by the sample thickness so that comparisons among samples in this study could be made on a relative basis. Additional information regarding the experimental setup is provided in the [Supporting Information](#).

3. RESULTS AND DISCUSSION

3.1. Blend Morphology. The PEO, PBO, and PEO-PBO additives were melt-blended with PLA at $\sim 5.0 \text{ wt } \%$ loading and compression-molded into films. [Figure 1](#) shows the SEM images of cryo-fractured film surfaces after rinsing with methanol. The cryo-fractured surface of the PEO/PLA blend

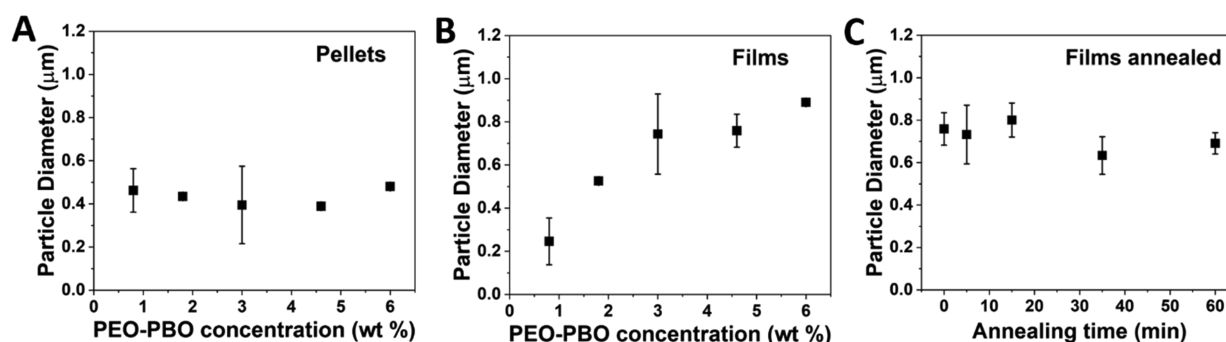


Figure 2. PEO-PBO particle sizes in PEO-PBO/PLA blends as a function of PEO-PBO concentration in (A) as-compounded pellets and (B) after compression molding into film samples at 135 °C for 5 min. (C) Particle size of 4.7 wt % PEO-PBO/PLA blend films after additional annealing at 135 °C following compression molding.

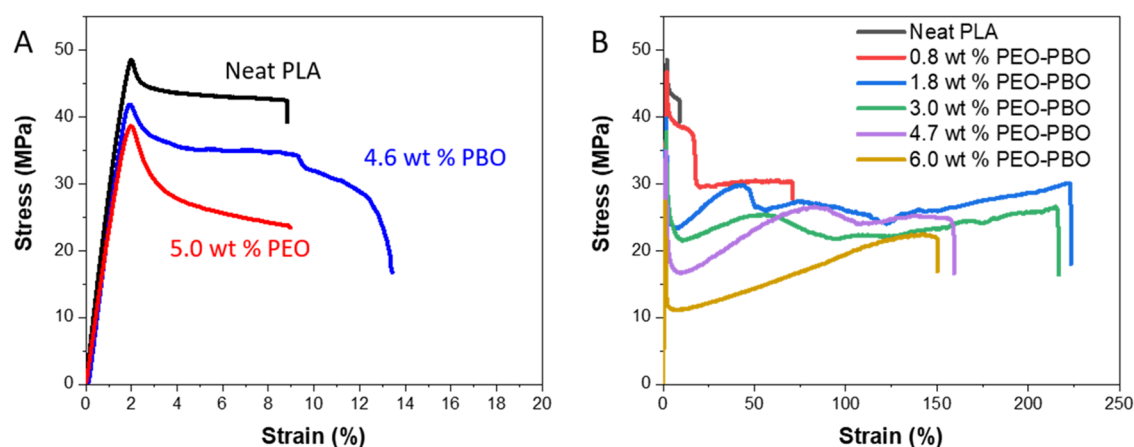


Figure 3. Representative stress–strain data of (A) PLA, PEO/PLA, and PBO/PLA blends at ~5 wt % loading and (B) PEO-PBO/PLA blends at various PEO-PBO concentrations. All stress–strain data are after aging at room temperature for 2 days.

(Figure 1A) was smooth and featureless, indicative of the molecular miscibility between PEO and PLA. This is consistent with a negative Flory–Huggins interaction parameter χ , which has been previously reported for the PEO/PLA pair.^{31,32} In contrast, Figure 1B,D shows large and nearly spherical voids for the PBO/PLA blend, with an average size of $1.8 \pm 0.2 \mu\text{m}$ and polydispersity of 3.1 ± 0.9 . We note that the SEM images of the cryo-fractured neat PLA film after methanol rinsing did not exhibit any void formation, confirming that the voids in the PBO/PLA blend correspond to the dispersed PBO particles after solvent extraction (Figure S3 in the Supporting Information). The macrophase-separated morphology of the PBO/PLA blend is consistent with their thermodynamic immiscibility.³⁹ Interestingly, Figure 1C,E shows that the average particle size in the PEO-PBO/PLA blend is $0.8 \pm 0.1 \mu\text{m}$ with a polydispersity of 1.3 ± 0.1 . We hypothesize that the reduction in particle size and dispersion (i.e., smaller size polydispersity) can be attributed to the miscible PEO block providing a compatibilizing effect. Although PEO-PBO still macrophase-separates as opposed to forming discrete micelles in PLA, the “PLA-philic” PEO block likely decreases the interfacial tension by favorable mixing with the PLA matrix, while the “PLA-phobic” PBO block mixes with the PEO-PBO dispersed phase that constitutes the liquid core of the particle. We expect that the “PLA-philic–phobic” diblock structure enables a lower critical capillary number for particle breakup that facilitates formation of a much smaller dispersed phase during melt processing.^{44,45} Overall, the unique molecular

structure of the PEO-PBO diblock copolymer leads to a liquid particle phase ($T_g \approx -70 \text{ }^\circ\text{C}$) that is well dispersed within the PLA matrix.

The effect of PEO-PBO concentration on the PEO-PBO/PLA blend morphology was further investigated before and after compression-molding pellets into films at 135 °C for 5 min. Interestingly, Figure 2A shows that the dispersed PEO-PBO particle size ($\sim 0.5 \mu\text{m}$) in PEO-PBO/PLA blend pellets remained constant, within experimental uncertainty, over concentrations of 0.8–6 wt %. In contrast to the precursor PEO-PBO/PLA blend pellets, Figure 2B shows that the particle sizes in the compression-molded films increase with PEO-PBO loading. The difference in particle sizes between blend pellet precursors and compression-molded films is likely a result of the kinematic balance between droplet breakup and coalescence during melt processing.³⁹ In the case of blend pellets, PEO-PBO droplets are constantly under high shear imposed by the twin-screw extruder, mitigating significant droplet coalescence in the melt state. The blend morphology can be mostly preserved since the extrudate is quickly quenched below the matrix T_g (56 °C) using a cooling water bath. In contrast, the compression-molded thin films can potentially undergo a higher degree of droplet coalescence in the melt state due to the limited amount of flow that occurs during compression molding. As the PEO-PBO loading increases, enlarged particle sizes are also promoted. The effect of additional annealing time on the blend film morphology was also investigated by monitoring the average particle size of the

Table 2. Summary of the Mechanical Properties of Neat PLA and PLA Blended with Various Additives^a

polymer blend	T_g (°C)	E (GPa)	σ_Y (MPa)	ϵ_Y (%)	σ_N (MPa)	ϵ_N (%)	ϵ_B (%)	toughness (MJ/m ³)
neat PLA	56	3.0 ± 0.1	51 ± 2	1.9 ± 0.1			9 ± 4	3 ± 2
5.0 wt % PEO	46	2.7 ± 0.1	39 ± 1	1.7 ± 0.1			10 ± 3	3 ± 1
4.6 wt % PBO	55	2.7 ± 0.1	37 ± 4	1.8 ± 0.2			17 ± 10	4 ± 3
0.8 wt % PEO-PBO	55	2.9 ± 0.1	45 ± 2	1.8 ± 0.1	36 ± 3	15 ± 4	74 ± 60	23 ± 20
1.8 wt % PEO-PBO	54	2.8 ± 0.1	40 ± 3	1.7 ± 0.1	29 ± 3	39 ± 7	221 ± 46	58 ± 11
3.0 wt % PEO-PBO	53	2.8 ± 0.1	35 ± 4	1.5 ± 0.2	24 ± 3	54 ± 4	201 ± 46	45 ± 12
4.7 wt % PEO-PBO	51	2.8 ± 0.1	34 ± 4	1.5 ± 0.2	24 ± 4	76 ± 6	159 ± 45	34 ± 12
6.0 wt % PEO-PBO	48	2.7 ± 0.1	28 ± 2	1.2 ± 0.1	22 ± 2	140 ± 5	148 ± 58	26 ± 13

^aThe \pm is one standard deviation about the mean, and 10 replicates were completed for each sample.

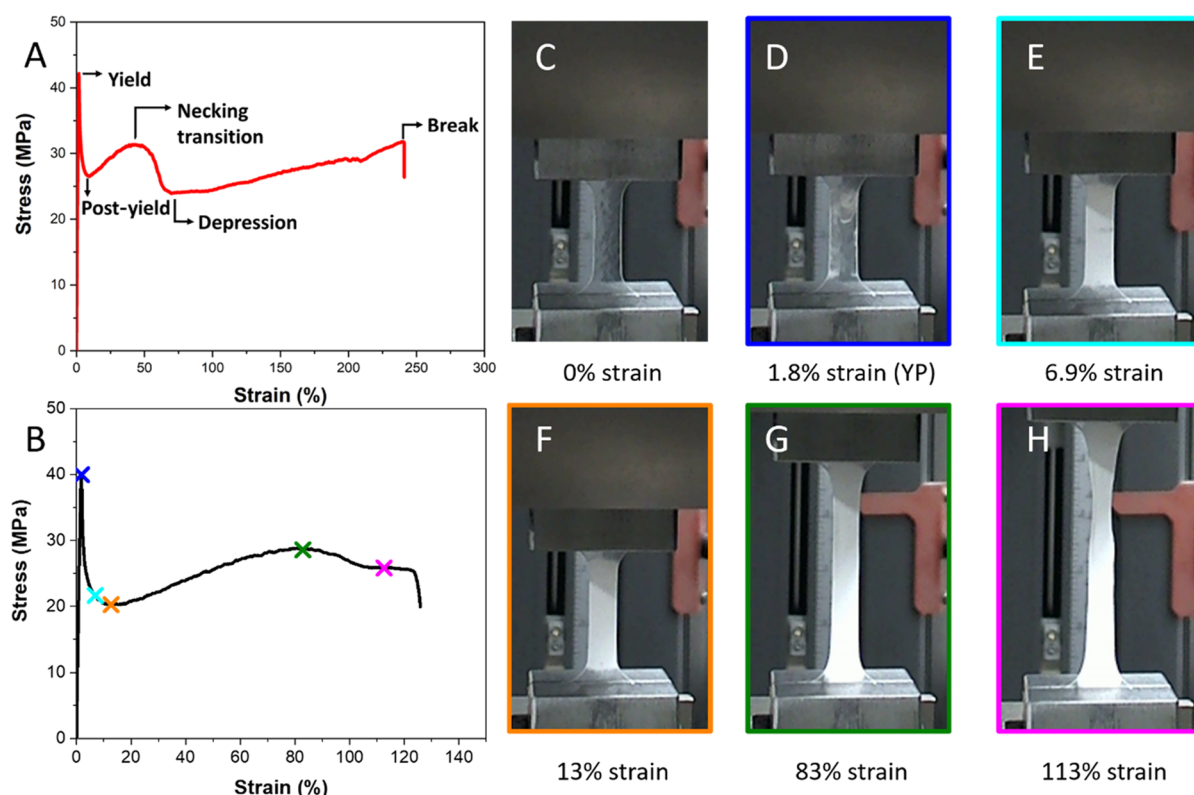


Figure 4. (A) Representative stress–strain data (from 1.8 wt % PEO-PBO/PLA blend) with features labeled for reference. (B) Representative stress–strain data from a 4.7 wt % PEO-PBO in PLA blend with (C–H) labeled gauge section images at specified strains. The colors of the X labels on (B) correspond to the gauge images. Sample was aged at room temperature for 2 days before testing.

4.7 wt % PEO-PBO in PLA sample with increasing annealing time at 135 °C (i.e., additional annealing following the initial 5 min of annealing during compression molding). As shown in Figure 2C, the particle size did not change as a function of additional annealing time, indicating that the particle size appears to be stabilized immediately after compression molding.

3.2. Mechanical Properties. Uniaxial tensile tests were performed on all samples after 2 days of physical aging at room temperature. Representative stress–strain data are shown in Figure 3, and the calculated mechanical properties are summarized in Table 2. As shown in Figure 3A, neat PLA exhibited a typical brittle behavior after 2 days of aging, characterized by elastic deformation with a Young's modulus (E) of 3 GPa, representative of the stiff nature of PLA, followed by yielding at a strain (ϵ_Y) of 1.9% with a yield stress (σ_Y) of 51 MPa then failing at an elongation at break (ϵ_B) of 9%. During elongation, the sample gauge area displayed a few small white horizontal streaks perpendicular to the tensile

direction (Figure S5). The orientation of these streaks indicates that they are likely the result of light scattering from voids formed from crazing.^{46,47} Addition of 5 wt % PEO or PBO to PLA resulted in blends that had similar toughness to that of neat PLA. The PEO/PLA gauge region behaved similar to neat PLA, forming a few small white horizontal streaks perpendicular to the tensile direction indicative of crazing. PEO is known to be miscible with PLA^{32–34} (also supported by Figure 1A), and it acts as a plasticizer, resulting in a decreased σ_Y (σ_Y = 39 MPa) compared to that of neat PLA. Previous research suggests that sufficient plasticizer must be added to reduce the PLA T_g below 35 °C to successfully toughen the plastic.^{13,36,48,49}

Table 2 shows that the 5 wt % PEO in the PLA blend had a T_g of 45 °C, which is insufficient to achieve this threshold. Blending 4.6 wt % PBO with PLA also resulted in a mechanically inferior material to PLA. A reduced σ_Y of 37 MPa compared to neat PLA coincided with complete whitening of the gauge region as a result of particle

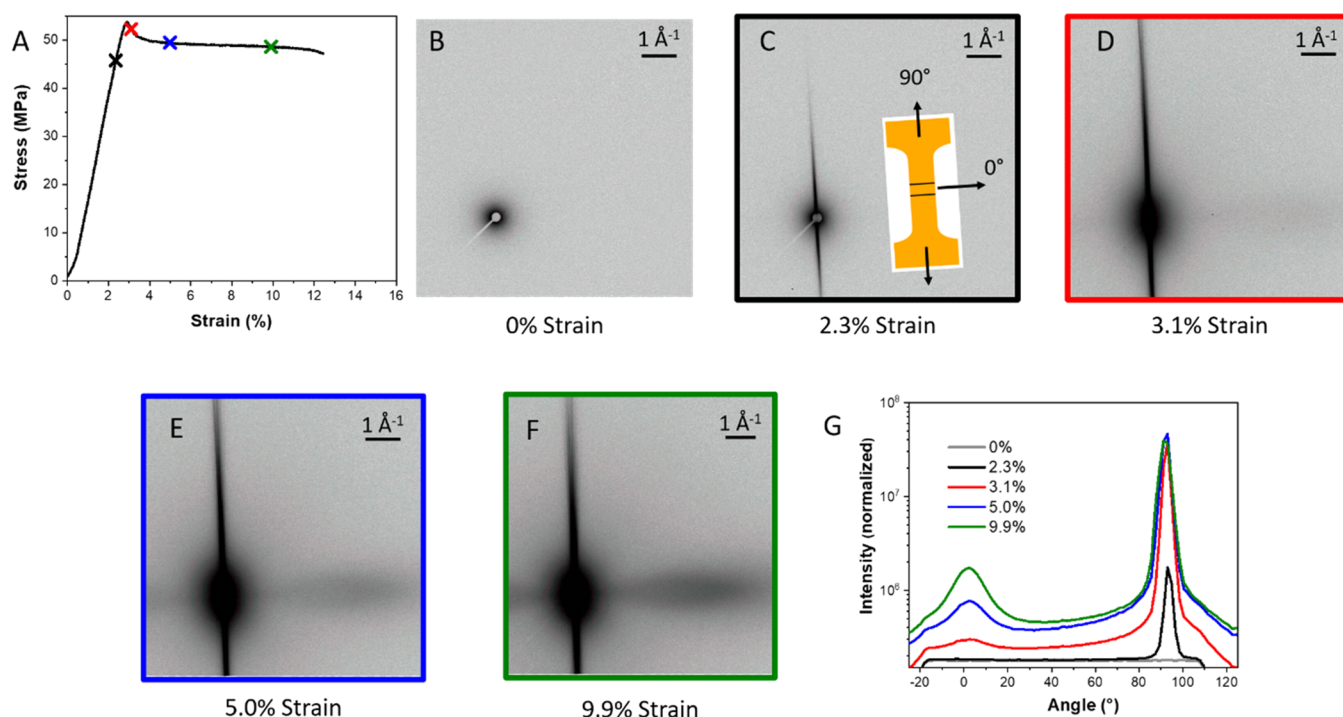


Figure 5. (A) Representative neat PLA tensile stress–strain data obtained during in situ tensile SAXS experiments with × symbols corresponding to (C–F) 2D SAXS patterns. The color of the × symbols in (A) indicates the corresponding 2D SAXS patterns. (G) 1D azimuthal angle vs intensity obtained from radial integration of 2D SAXS patterns. The neat PLA sample was aged for 2 days.

cavitation.^{50,51} However, the tensile bar failed shortly after passing the yield point. We attribute this early failure to the relatively large PBO particle sizes, which can lead to large micron-sized cavities that cause catastrophic cracks and failure.^{51,52}

In stark contrast, Figure 3B shows that the PEO-PBO/PLA blends displayed dramatically improved ductility and exhibited additional stress–strain features. These features, including yielding, post-yield stress reduction, necking transition, stress depression, and breaking, are labeled in Figure 4A and are discussed below in more detail. For better visual illustration, the deformation of a tensile bar during extension, representative stress–strain data, and corresponding images of the gauge area from a 4.7 wt % PEO-PBO in PLA blend are provided in Figure 4B–H. Similar to neat PLA, the first characteristic feature in the PEO-PBO/PLA blend stress–strain data is the yield point. The yield stress σ_Y and yield strain ϵ_Y for the PEO-PBO/PLA blends were lower than σ_Y and ϵ_Y for neat PLA (Figure 4B and Table 2). At the yield point, the initially clear gauge region (Figure 4C) began to whiten (Figure 4D), indicative of void formation.^{46,47} This is due to particle cavitation or craze formation, which is considered in more detail in a later section. After the yield point, the stress decreased quickly to a minimum value, during which the gauge region continued to whiten (i.e., voids continued to form; Figure 4E). When the stress minimum was reached, the gauge region was completely whitened and opaque (Figure 4F). Upon further elongation, the material exhibited strain hardening. We attribute this stress increase to the orientation of the polymer chains in the craze fibrils. From the start of the test until the necking transition, the material deformed uniformly throughout the entire gauge section where the width and thickness remained essentially constant (Figure 4G). Therefore, volume expansion due to voiding within the

specimen accompanies the deformation, indicating that crazing is the main deformation mechanism.⁵³ As the stress further increased, the specimen approached the flow stress at the necking transition, where the sample thickness and width decreased in a localized region of the gauge section (Figure 4H). We hypothesize that the deformation mechanism at the necking transition changes due to macroscopic changes in the sample. From the point of necking to failure, the sample underwent cold drawing and the neck propagated throughout the gauge region.

Based on the results in Figure 3 and Table 2, the concentration of PEO-PBO in PLA has a significant effect on the mechanical properties. E decreased with increasing amount of PEO-PBO, consistent with previous studies;^{51,54,55} however, even at the highest examined loading, i.e., 6 wt % PEO-PBO in PLA, the modulus was within 90% of neat PLA. Similarly, σ_Y and ϵ_Y decreased as the loading of PEO-PBO increased, a result of the liquid particles formed by PEO-PBO in the PLA matrix. The liquid particles can act as stress concentrators due to their lower compliance compared to the PLA matrix, allowing the blend to yield at a lower applied stress.^{56,57} As the particle volume fraction increases, naturally so does the density of stress concentrators.^{25,51,57,58} In addition, the stress at the necking transition (σ_N) decreased while the necking transition strain (ϵ_N) increased as a function of PEO-PBO concentration. With increasing PEO-PBO loading, the stress required for material flow during/after extensive crazing decreased. The PEO-PBO partially plasticizes PLA, which is evident from the slight decrease in T_g with increasing PEO-PBO loading (Table 2). Moreover, the ϵ_N increased with PEO-PBO loading due to the increase in particle surface area, which leads to an increase in crazing and energy dissipation. Therefore, the material must be elongated to larger strains during strain hardening to reach the necessary

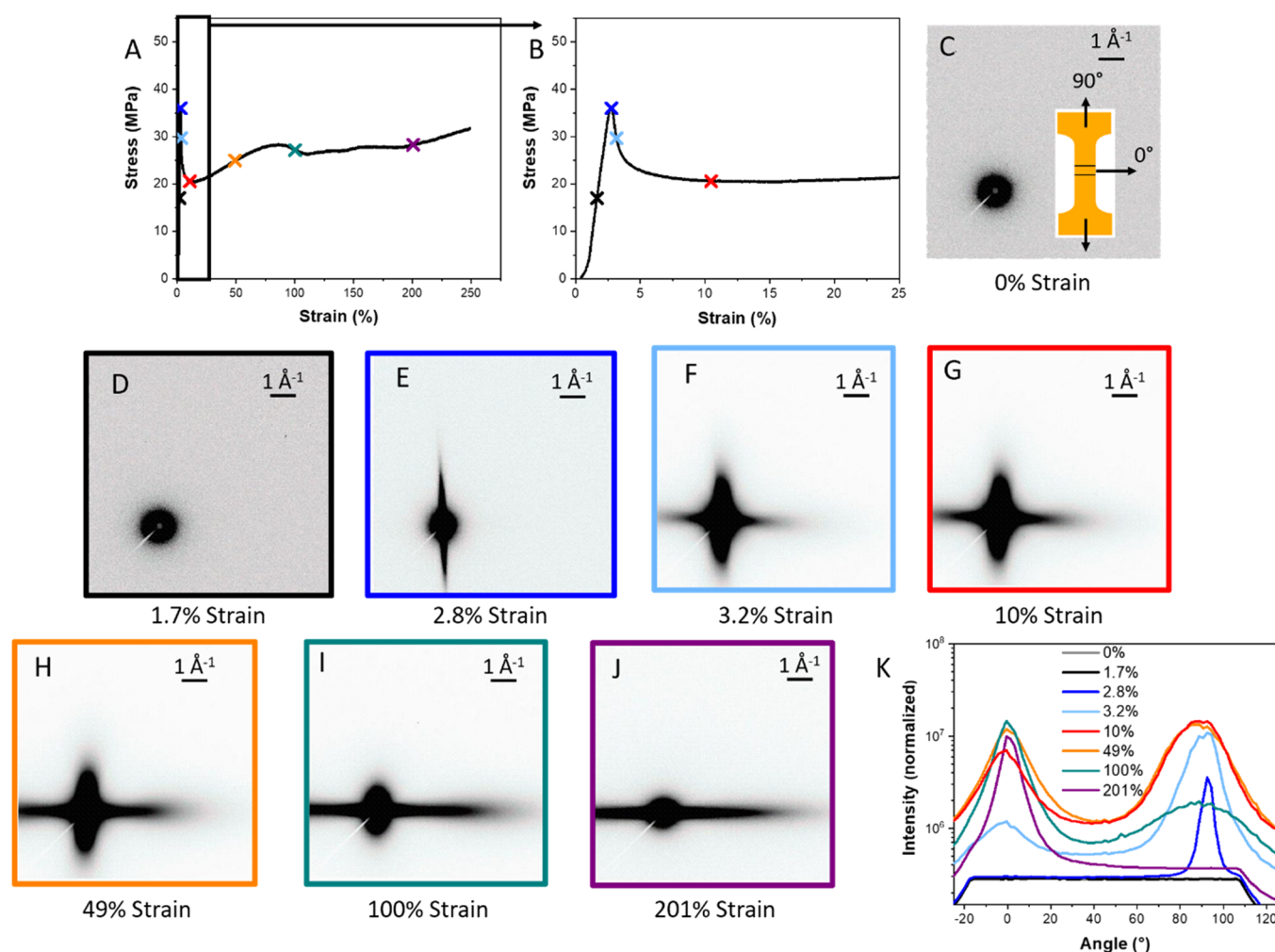


Figure 6. (A) Representative tensile stress–strain data acquired from in situ tensile SAXS for 4.7 wt % PEO-PBO in PLA. (B) Zoom-in view of (A) at low strain (0–25% strain) to reveal the low-strain tensile properties. The color of the × labels on (A) and (B) corresponds to the border of the (D–J) 2D SAXS patterns. (K) 1D SAXS plot of azimuthal angle vs intensity constructed from radial integration of 2D SAXS patterns. The sample was aged for 2 days.

flow stress to initiate necking. The strain at break (ϵ_B) and toughness (i.e., integrated area under the stress–strain data⁵⁹) did not follow a linear trend. In fact, the blend ϵ_B peaked at 1.8 wt % PEO-PBO in PLA (~20-fold increase compared to neat PLA) and finally decreased as more PEO-PBO was added (~10-fold increase at 6.0 wt % PEO-PBO in PLA compared to neat PLA). The increase in PEO-PBO loading leads to a greater particle surface area (i.e., greater stress concentrator area for crazing), resulting in a larger fraction of the test specimen volume engaging in the crazing process. This increases the chances for craze fibril breakdown due to thickening crazes intersecting with inhomogeneities in the sample (i.e., dust particles or isolated cavitated particles) or due to craze impingement;⁶⁰ as crazes thicken, they will intersect and destabilize one another. Once one fibril fails, the stress increases on the neighboring fibrils and causes multiple fibril failure, resulting in a crack that leads to early failure.

Based on the results from the tensile tests and SEM morphologies of the PEO-PBO/PLA, PEO/PLA, and PBO/PLA blends, it is evident that both components in the diblock copolymer are essential to achieve the necessary particle size to toughen PLA. In the PEO-PBO/PLA blend, the PBO immiscibility leads to macrophase separation and particle

formation due to unfavorable enthalpic interactions between PBO and PLA, while the enthalpically favorable PEO/PLA interactions lower the interfacial energy, leading to a decreased and controlled particle size (tunable by varying the chemical details of PEO-PBO). In the PLA matrix, the PEO-PBO diblock copolymers assemble into particles within an ideal size range,^{4,27,28} which can stably cavitate and then act as stress concentrators to effectively toughen PLA.

3.3. Toughening Mechanism of the PEO-PBO/PLA Blends. The discussion in the previous sections has provided a rather macroscopic view of the PEO-PBO/PLA blend deformation behavior and the toughening effects brought by PEO-PBO. In this section, we aim to gain more fundamental insight into the deformation mechanisms behind the toughening enhancements at the microscopic level. To achieve this goal, in situ SAXS experiments were performed during tensile tests to probe the craze fibril development during elongation.^{61–65} Comprehensive experimental details and specifications are provided in the [Supporting Information](#). We note that the tensile specimens for in situ SAXS measurements were elongated at the same rate as those used for regular tensile tests (Figures 3 and 4 and Table 2). All specimens for in situ SAXS measurements were also aged for 2

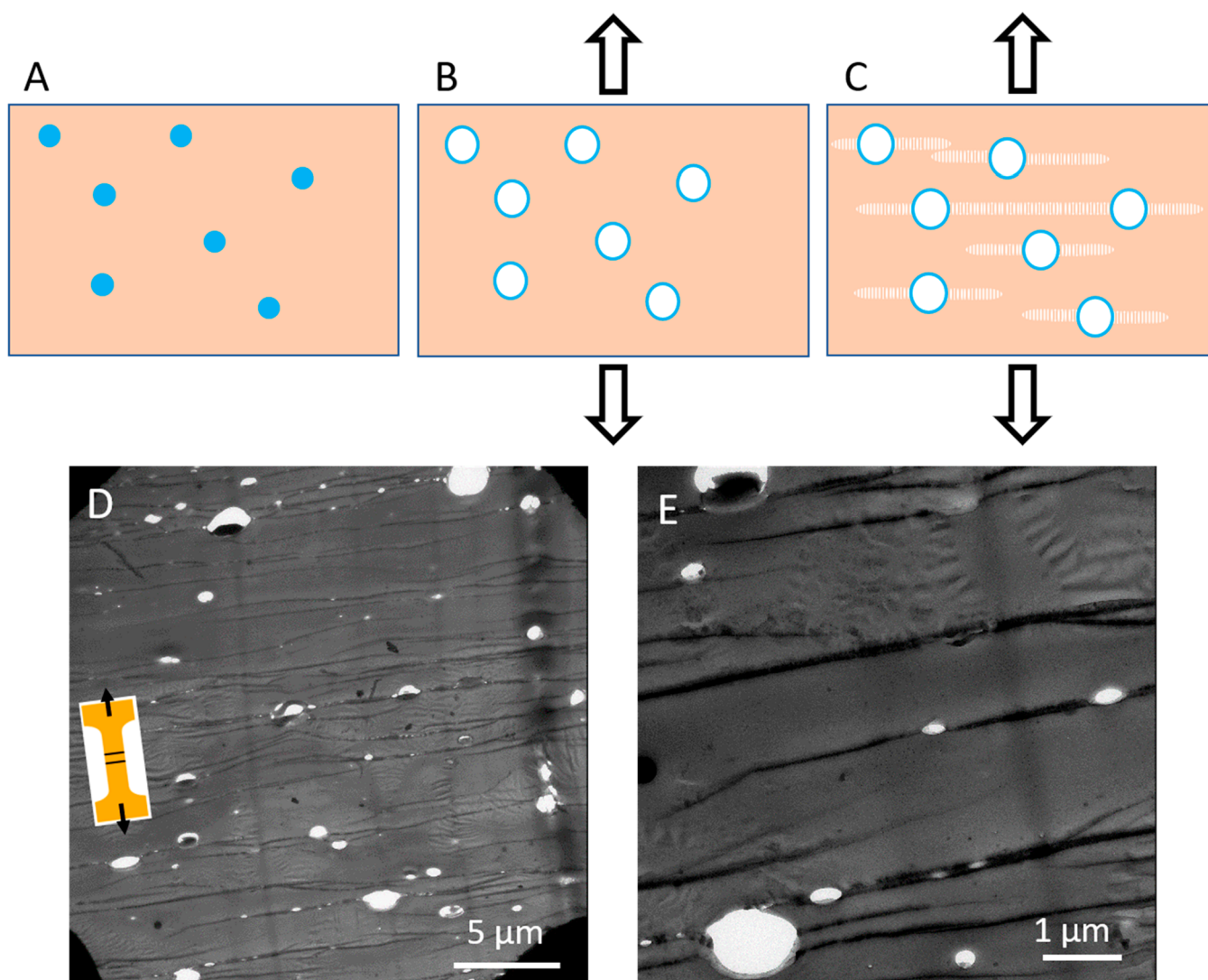


Figure 7. Schematic of (A) PEO-PBO particles (blue circles) in the PLA matrix (orange) before deformation (0% strain). (B) Cavitation of PEO-PBO particles during tensile deformation. (C) Craze initiation and growth from the cavitated particles as the material is strained further. (D and E) TEM images of the gauge region of a 4.7 wt % PEO-PBO in PLA sample at 10% strain taken at different magnifications. Samples were stained with RuO_4 .

days at room temperature, and they exhibited a stress–strain behavior nearly identical to those obtained in Figure 3.

3.3.1. Deformation Mechanism of PLA. The in situ tensile SAXS data for neat PLA yield several different key pieces of information, with each referenced to its in situ stress–strain behavior shown in Figure 5A. Two-dimensional SAXS patterns (Figure 5B–F) are used for qualitative comparison between neat PLA and the PEO-PBO/PLA blends (see the next section), while the azimuthal angle vs intensity (I) data (Figure 5G) provide a quantitative assessment of the scattering results. During deformation, the 2D SAXS pattern of neat PLA remained featureless until just before the yield point at $\sim 2.3\%$ strain (Figure 5C), where a sharp increase in scattering intensity at 90° , i.e., along the tensile direction (meridional axis), was observed (as shown in Figure 5G), indicative of void formation within the sample.⁶⁶ These voids are likely initiated by impurities in the PLA matrix such as dust particles and residual catalysts.^{46,47} Due to the inhomogeneous distribution of these defects, the strain is localized and therefore additional deformation is necessary before the material can yield. As the

material is further elongated and more voids are formed, the meridional streak intensified until it plateaued at 3.1% strain (Figure 5D–F). At 3.1% strain, there was a slight increase in intensity at 0° (Figure 5D), i.e., perpendicular to the tensile direction (equatorial axis), which also can be seen in Figure 5G. This increase in scattering intensity is due to the contrast between the newly formed craze fibrils and void space.^{61,66,67} Because of the limited volume fraction associated with the voids and crazes in neat PLA, the associated strain and stress are highly localized. The locally deformed material can be elongated at a lower stress than the undeformed surrounding material, and hence strain localization is further enhanced, leading to early failure. The normalized equatorial intensity continued to increase and reached a maximum value before failure. Notably, the equatorial intensity is proportional to the craze volume, which is discussed below in more detail.

3.3.2. Deformation Mechanism of PEO-PBO/PLA Blends. In situ tensile tests with SAXS were performed on all PEO-PBO/PLA blends with various PEO-PBO loadings. The 4.7 wt % PEO-PBO in PLA blend is used as a representative example

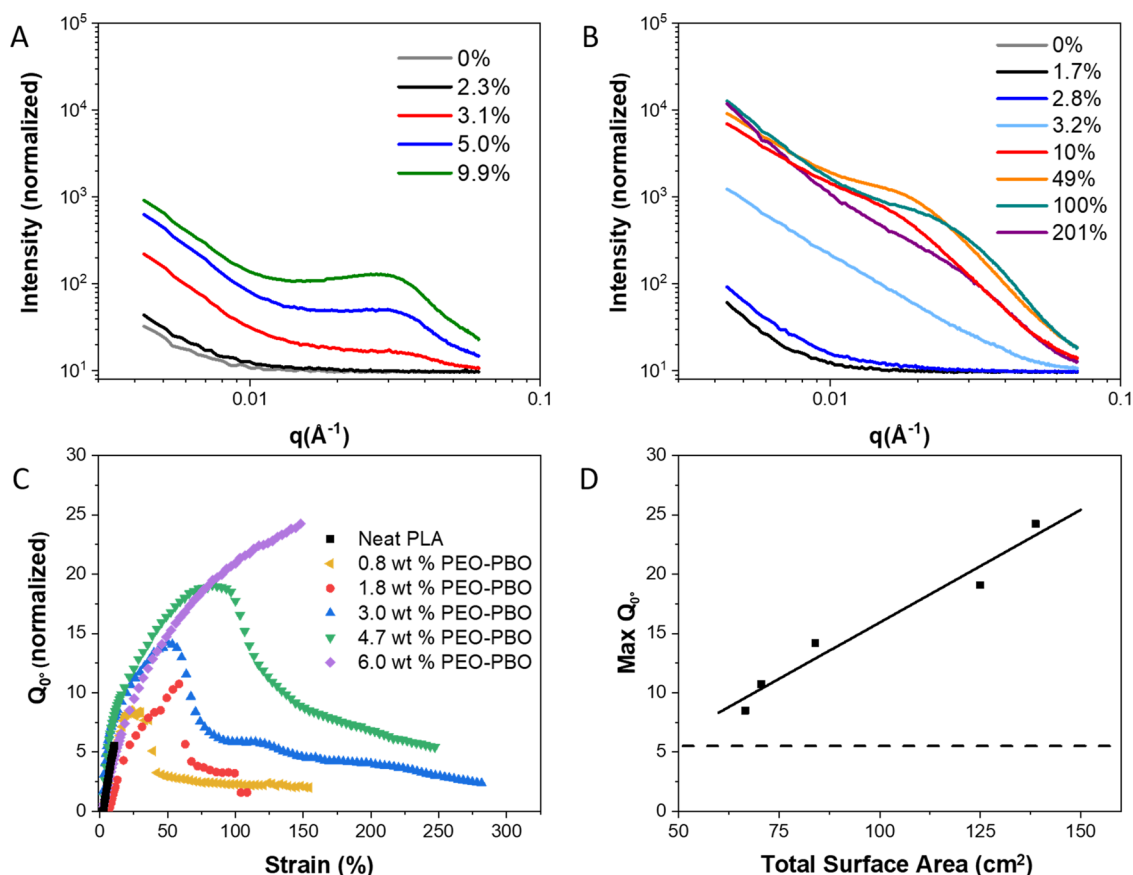


Figure 8. 1D SAXS patterns obtained by integration of the intensity between azimuthal angles of -10° to 10° for (A) neat PLA and (B) 4.7 wt % PEO-PBO in PLA. (C) Plot of invariant (Q_0) vs strain for various wt % PEO-PBO in PLA using the intensity normalized by sample thickness. (D) Maximum (Max) invariant Q_0 from (C) vs total particle surface area (which is equal to the surface area of an average-sized particle times the average number of particles in the gauge area) for PEO-PBO/PLA blends (solid line is a linear fit of the data). The dotted line represents the Q_0 of neat PLA. All samples were aged for 2 days before testing.

to discuss the blend stress–strain behavior and corresponding microstructural evolution as compared to neat PLA. The stress–strain data (Figure 6A,B), 2D SAXS patterns at various strains (Figure 6C–I), and plot of azimuthal angle vs I (Figure 6J) are displayed in the indicated figures. The PEO-PBO particles are too large to generate form-factor scattering that can be detected by SAXS. Therefore, the observed scattering should reflect particle-based Porod scattering ($I \sim q^{-4}$) and scattering from voids associated with cavitated particles and crazes. The much larger electron density difference between voids and the polymer, versus PEO-PBO and PLA, means that the former will dominate the experimental scattering profiles.

All the 2D SAXS patterns obtained from the 4.7 wt % PEO-PBO in PLA blend in the elastic regime ($\epsilon < 0.028$) were identical to those recorded at 0% strain (Figure 6C,D). At the yield point, there was a sharp increase in scattering along the meridional axis, indicative of void formation (Figure 6E,K). The void formation for all the PEO-PBO/PLA blends occurs either at or slightly beyond the yield point, never prior to yielding as is the case for neat PLA. Yielding is accompanied by particle cavitation and subsequent void expansion, which relieves stress in the matrix and a reduction in the measured stress after the yield point.^{52,68} Following the yield point, at 3.2% strain, there was a sharp increase in the scattering intensity in the equatorial axis (Figure 6F,K), indicative of craze fibril formation. According to Figure 6K, the intensity due to crazing along the 0° axis is much greater for the 4.7 wt

% PEO-PBO in PLA blend than for the neat PLA due to the presence of liquid particles. These well-dispersed particles can act as craze-initiating sites that allow crazes to grow in a controlled manner throughout the entire sample, dissipating energy by craze fibril formation. These conclusions are further supported by TEM images obtained from elongated tensile bars, as displayed in Figure 7. A 4.7 wt % PEO-PBO in PLA sample was elongated to 10% strain and removed for TEM preparation. TEM images reveal that there are voids, about the same size as or slightly larger than the particles (~ 800 nm in diameter), distributed throughout the sample due to cavitated particles with crazes extending from the voids perpendicular to the tensile direction. The scattering intensity in the equatorial region continually increased until about 100% strain (Figure 6I), at which point a maximum value of approximately 10 times that of neat PLA was reached. At 100% strain, the equatorial scattering intensity reached a plateau, signaling cessation of craze fibril formation and a change in the toughening mechanism from crazing to shear yielding (i.e., material flow). At 201% strain, the scattering intensities in both the meridional and equatorial directions decreased (Figure 6J,K), which is likely due to necking, leading to a decreased sample thickness and scattering volume.

Based on the in situ tensile SAXS results, both neat PLA and the PEO-PBO/PLA blends form crazes when elongated. The neat PLA sample develops a limited number of voids before the yield point and then grows crazes in a few localized areas as

the material is extended to failure. In comparison, the well-dispersed particles (stress concentrators) in the PEO-PBO/PLA blends act as craze-initiating sites, leading to the development of numerous crazes uniformly throughout the entire material, adsorbing energy and blunting crack formation.

3.3.3. Influence of PEO-PBO Loading on Craze Development. Although all the PEO-PBO/PLA blends exhibited similar stress–strain characteristics, they differed in craze development and the portion of the gauge volume engaged in crazing. To analyze the crazes formed in neat PLA and PEO-PBO/PLA blends, the invariant of the X-ray scattering along the equatorial (0° azimuthal angle) axis (Q_{0°) was calculated by integration of the 1D q vs I SAXS plots (Figure 8A,B) according to⁶⁹

$$Q_{0^\circ} = \int_0^\infty I(q) \times q^2 \times dq \quad (1)$$

The invariant is related to the volume of crazes (V) and fibril volume fraction in a craze (v_f)

$$Q_{0^\circ} = Vv_f(1 - v_f)\Delta\rho^2 \quad (2)$$

where $\Delta\rho$ is the electron density difference between the polymer and void space. We note that eq 1 differs from that reported by Kramer and Brown⁶¹ due to differences in the experimental setup. Here, SAXS experiments were performed with a pinhole geometry, while Kramer and Brown used a slit geometry. Assuming v_f has limited variability at low concentrations (<10 wt %) of PEO-PBO^{69,70} and $\Delta\rho$ is a constant for all blends, the changes in Q_{0° are directly related to V . Q_{0° is plotted versus strain for the five PEO-PBO concentrations in Figure 8C. The maximum Q_{0° values at each block copolymer loading are plotted against the total surface area of particles (i.e., product of the surface area of one particle times the total number of particles in the gauge region) in Figure 8D, resulting in a linear fit. The total craze volume (V) is linearly dependent on the particle surface area due to the fact that crazes are initiated at the void/polymer interface. With increasing V , a greater strain is required to reach the necessary flow stress for necking to occur, thus increasing ϵ_N . This is due to increased energy dissipation from craze formation and an increase in load-bearing fibrils, resulting in greater fibril stability. It is also worth noting that, with increasing PEO-PBO concentration, both Q_{0° and the strain at which Q_{0° reaches a maximum (ϵ_M) increased (Figure 8C), while ϵ_M coincided with ϵ_N for all the PEO-PBO/PLA blends. Q_{0° leveling off or decreasing at ϵ_M provides additional evidence that at ϵ_N , the deformation mechanism changes from crazing to shear yielding as the material necks.

3.3.4. Effect of the PEO-PBO Particle Size. The PEO-PBO particle size also impacts the stress required for craze initiation. From the in situ SAXS data obtained during tensile testing, the craze initiation stress (σ_{1cz}) can be determined as the stress at which the intensity at an azimuthal angle of 0° is 5% greater than the baseline intensity in the azimuthal angle vs I plot (neat PLA in Figure 5G and blends in Figure 6J). Figure 9 shows σ_{1cz} vs average diameter of the dispersed PEO-PBO particles in PLA. The σ_{1cz} for neat PLA is 50 MPa, which is within the typical stress range seen in the literature,^{71,72} while σ_{1cz} decreased by $\sim 50\%$ to 26 MPa upon blending 3 wt % PEO-PBO with PLA. As a crack approaches a particle, a larger sample volume can initiate a craze due to the decreased σ_{1cz} .^{16,45} As the material begins to deform and dissipate energy

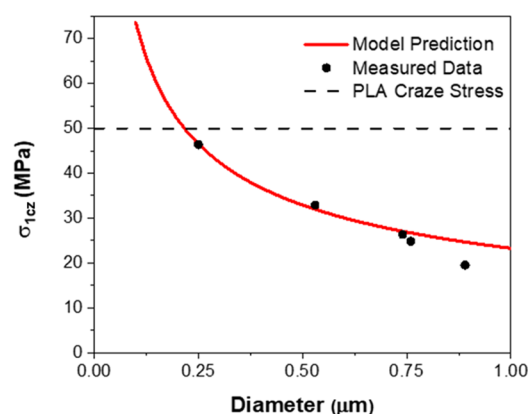


Figure 9. σ_{1cz} vs diameter data, along with model predictions from eq 3 (solid line) and neat PLA craze stress (dashed line). All data were recorded after aging tensile bars at room temperature for 2 days.

at lower stresses, additional strain is required to reach the craze fibril breakdown stress (fibril failure), leading to greater toughness. Craze initiation can be modeled as linear elastic fracture with a crack of length D .^{16,45} The relationship between σ_{1cz} and D can be described using a modified Griffith equation⁷³ as proposed by Bucknall^{56,74}

$$\sigma_{1cz} = \sqrt{\frac{\pi E G_{1cz}}{2(1 - \nu)^2 D}} \quad (3)$$

where E is the elastic modulus, G_{1cz} is the specific work done in creating a unit area of new craze, and ν is the Poisson ratio. σ_{1cz} calculated with eq 3 using the material parameters for PLA ($E = 3.0$ GPa, $\nu = 0.35$,⁷⁵ and $G_{1cz} = 0.1$ J/m²; see the Supporting Information for the detailed calculations and assumptions) is plotted versus diameter in Figure 9.^{56,74} This plot reveals that the PEO-PBO/PLA blend results follow the model predictions closely at smaller PEO-PBO particle diameters (corresponding to lower PEO-PBO loading). This provides evidence supporting the notion that craze initiation resembles linear elastic fracture mechanics as opposed to yielding, which other researchers^{76–78} have employed to model craze initiation. Modest deviation from the observed data at larger PEO-PBO particle diameters (>0.75 μm, or higher loading) is due to the cavitation of PEO-PBO particles, leading to a porous material. Therefore, the average stress in the matrix becomes greater than the applied stress. Another potential source for the deviation is the decrease in E , which was taken to be a constant, with increasing PEO-PBO loading. Although crazing can be modeled by a linear elastic fracture mechanism, catastrophic failure is avoided due to the reinforcement mechanism of fibril formation.^{56,74,79,80}

The craze fibril spacing is a key factor dictating how the craze propagates perpendicular to the tensile direction. The broad peaks at high q in Figure 8A,B are associated with the inter-fibril scattering, and the peak can be used to estimate the craze fibril spacing ($D_0 = 2\pi / q_{\max}$).^{61,81–83} The calculated D_0 values of neat PLA are all around 20 nm, independent of strain and similar to those obtained by the same analysis for polystyrene⁸⁴ ($D_0 = 30$ nm). The estimated D_0 values are plotted against strain for each PEO-PBO/PLA blend and compared to that for neat PLA in Figure 10. There are two clear trends observed in Figure 10: the fibril spacing (1)

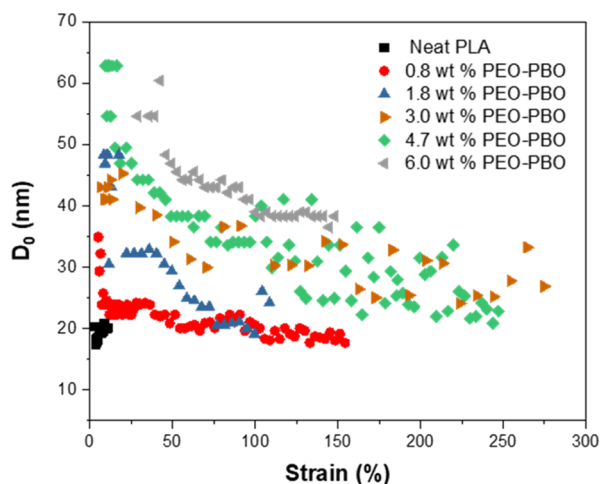


Figure 10. Craze fibril spacing (D_0) as a function of strain. All data were recorded after aging tensile bars at room temperature for 2 days.

increases as the PEO-PBO loading increases and (2) decreases with increasing strain. The fibril spacing can be expressed by⁸³

$$D_0 = \frac{8\Gamma}{\beta S} \quad (4)$$

where Γ is the energy to form a new craze surface, β is an $O(1)$ geometric constant, and S is the tensile stress at the craze interface. It is generally accepted that for a given system, D_0S is a constant, therefore $8\Gamma/\beta$ in eq 4 will be treated as a constant.^{83,85,86} With increasing PEO-PBO loading, D_0 increases, resulting in decreasing fibril stress. A lower fibril stress leads to crazes occurring and propagating at lower stresses. This is likely a result of the lower T_g of the material with increasing PEO-PBO loading.^{70,84,87} A lower S contributes to the increase in ϵ_N that is observed with increasing PEO-PBO loading (Table 2). When the stress on the fibrils is lowered, the fibrils can be extended to greater elongations before the flow/breakdown stress is reached.

Interestingly, the fibril spacing also is observed to decrease as the material is elongated. For this to happen, the craze fibrils must have become closer to one another as the tensile bar was extended because this observation cannot be the result of new fibrils developing between the already formed craze fibrils as the craze continually thickens (along the tensile direction). Although the reason for such a decrease of craze fibril spacing is not fully understood, the results suggest a narrowing of the craze width (perpendicular to the strain direction), thus compressing the fibrils. This trend provides evidence of the craze fibril stability. The fibrils are initiated at low strains ($\sim 3\%$) and continue to develop up to 70% strain in some samples. As the material extends, the craze fibril spacing decreases, indicating that the fibrils are not breaking (which would otherwise lead to an increase in D_0). The increase in PEO-PBO concentration allows for the crazes to propagate at lower stresses, and the crazes appear to be stably thickened (along the strain direction), avoiding fibril failure until fracture.

It is worth noting that although other researchers have observed rubber particle cavitation induced plastic deformation, the deformation seen was shear yielding.^{88–90} These differences arise due to variations in the testing conditions,⁹¹ sample aging time,^{92,93} particle size/morphology,^{28,74} and matrix crystallinity.²⁸

Overall, the well-dispersed rubber particles in the PEO-PBO/PLA blends act as craze-initiating sites that facilitate crazes to develop uniformly throughout the material. The PEO-PBO concentration affects both the craze initiation and propagation stress, ultimately dictating the total craze volume and final material toughness.

3.4. Mechanical Properties as a Function of Physical Aging. All the data displayed to this point represent the behavior of neat PLA and PEO-PBO/PLA blends at 2 days of physical aging at room temperature. There are a variety of ways to study physical aging of a polymer. Common methods include (1) measuring enthalpy relaxation,^{10,94,95} (2) evaluating tensile mechanical properties,^{92,95,96} and (3) assessing low strain torsion creep.^{94,95} We have opted to monitor the physical aging of PLA in this work by examining the mechanical properties in tension, which we view as most directly relevant to applications. Few studies^{9,38,97–99} have examined the effectiveness of additives at longer aging times, and the effects of aging time on the deformation mechanism have been rarely investigated.⁹ Here, we examine the blends at longer aging times to ascertain the impact of physical aging on the deformation mechanism.

When polymers are processed as melts and then rapidly cooled below T_g , the chain segments are trapped in a metastable state with excess free volume.^{7,8,12,100} In an attempt to approach equilibrium, the chain segments undergo local relaxations, which lower the free volume, causing densification; this is called physical aging.^{100,101} With densification, polymer segment–segment interactions increase, making it more difficult for chains to move past one another.^{7,9,102} As a result, both E and σ_Y typically increase while ϵ_B decreases with aging. In contrast, crazing is directly related to the matrix entanglement density, which is independent of physical aging.⁸³ The craze stress usually remains constant and is eventually surpassed by the σ_Y as glassy polymers age.^{92,93,103–105} In homopolymers, craze deformation coincides with strain localization, leading to brittle failure.¹⁰⁵ Based on our earlier results, the main toughening mechanism of the PEO-PBO/PLA blends is uniform craze formation throughout the entire sample. Therefore, we hypothesize that these blends will remain ductile because the crazing stress does not change as a function of aging time, which is the subject of this section.

To test this hypothesis, the mechanical properties of the PEO-PBO/PLA blends were examined as a function of aging time at room temperature. Figure 11 displays representative stress–strain data from the 1.8 wt % PEO-PBO in PLA material with increasing aging time at room temperature, and Table 3 compiles the tensile test results for all the blend compositions. As the PEO-PBO/PLA blends aged at room temperature, for up to 114 days, the samples remained relatively tough compared to neat PLA. There are two general trends exhibited by the data: (1) ϵ_N increased and (2) ϵ_B decreased with increasing aging time. ϵ_N increases as a function of aging time due to the increase in flow stress as the material densifies. Therefore, the material must be extended to a greater strain to reach a higher flow stress as the plastic strain hardens. As the flow stress further increases, it will eventually exceed the critical stress that the craze fibrils can withstand, leading to craze fibril breakup and failure before necking can occur, and thus ϵ_B approaches ϵ_N . However, as the material continues to age, the ϵ_N of samples aged for 114 days eventually surpasses ϵ_B of samples aged for a shorter time (<114 days). Haugan et al.⁹ observed an increase in crazing and an increase in strain at

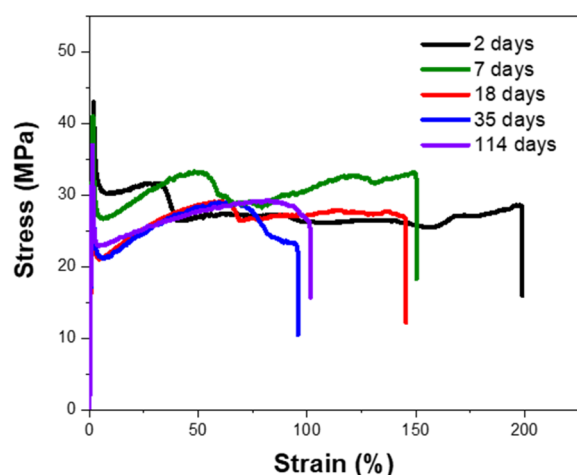


Figure 11. Representative stress–strain data for 1.8 wt % PEO-PBO in PLA at various aging times.

which necking and shear deformation occurred (ϵ_N) in PLA-based graft block polymers. They also identified similar trends in ϵ_B and ϵ_N . However, the PEO-PBO/PLA blends remain relatively tough with aging due to the high ϵ_N , reaching strains >80% for the PEO-PBO blends with 1.8 wt % and higher PEO-PBO loadings.

3.4.1. Craze Fibril Development as a Function of Time.

The craze stress is not associated with a yielding mechanism as discussed earlier and therefore is unaffected by the physical aging of the PLA matrix.^{92,93,103} Thus, the mechanical properties of the blends are expected to remain unchanged as the material ages, from 0% strain to ϵ_N . This is examined in Figure 12A using the invariant of the equatorial axis scattering intensity. The 4.7 wt % PEO-PBO in PLA blend was analyzed after aging for 2 and 30 days. Q_0 vs strain for both materials are very similar, where Q_0 increases rapidly between 10 and

50% strain before reaching a similar maximum value. This demonstrates analogous craze development and growth between these two samples and indicates that both samples have a similar number of total crazes and crazed volume.

Similar to Q_0 , σ_{1cz} and D_0 of the 4.7 wt % PEO-PBO in PLA blend can be examined as a function of aging time at room temperature to further investigate the effects of physical aging on the development of crazes. The σ_{1cz} of the 4.7 wt % PEO-PBO in PLA blend after aging for 2 days was 25 MPa, almost identical to that of the sample after aging for 30 days, i.e., 24 MPa. This confirms that σ_{1cz} does not change as a function of aging time, and crazing can initiate at the same stress at a given particle size. D_0 vs strain data for the 4.7 wt % PEO-PBO in PLA blend after aging at room temperature for 2 and 30 days are plotted in Figure 12B. Here again, the aged sample resembles the unaged sample, which provides further evidence that craze formation and development are unaffected by physical aging. Given that D_0S is a constant, we can conclude that S does not change as a function of aging, indicating that the crazes can propagate at the same stress values independent of aging time. Therefore, the decrease in ϵ_B can be attributed to the increase in yield stress as the material ages. However, the sustained toughness is a result of the invariant development of crazes as the material ages.

4. CONCLUSIONS

Detailed studies of the mechanical properties of PLA blends revealed the effectiveness of a commercial PEO-PBO diblock copolymer in toughening commercial PLA. We have demonstrated that individually, neither PEO nor PBO is able to toughen PLA. The diblock copolymer architecture is essential for the blend to assemble into a stable macrophase-separated particle morphology with ideal particle sizes that result in a tough blend. Optical transparency and efficacy at low PEO-PBO mass loading (1.8 wt %) further demonstrate

Table 3. Mechanical Properties of Neat PLA and PEO-PBO/PLA Blends at Various Aging Times^a

polymer blend	aging days	E (GPa)	σ_Y (MPa)	ϵ_Y (%)	σ_N^b (MPa)	ϵ_N^b (%)	ϵ_B (%)	toughness (MJ/m ³)
neat PLA	2	3.0 ± 0.1	50 ± 2	1.9 ± 0.1			9 ± 4	3 ± 2
0.8 wt % PEO-PBO	2	2.9 ± 0.1	45 ± 2	1.8 ± 0.1	36 ± 3	15 ± 4	74 ± 60	23 ± 20
	7	3.1 ± 0.1	49 ± 2	1.9 ± 0.1	38 ± 2	38 ± 2	47 ± 11	17 ± 4
	18	3.0 ± 0.2	45 ± 2	1.7 ± 0.1	32 ± 2	42 ± 2	35 ± 9	12 ± 2
	35	3.1 ± 0.1	46 ± 5	1.8 ± 0.2	42 ± 1	43 ± 2	53 ± 29	20 ± 11
	114	3.0 ± 0.1	43 ± 2	1.6 ± 0.1	36 ± 2	35 ± 2	96 ± 38	31 ± 13
1.8 wt % PEO-PBO	2	2.8 ± 0.1	40 ± 3	1.7 ± 0.1	29 ± 3	39 ± 7	221 ± 46	58 ± 11
	7	3.0 ± 0.1	42 ± 2	1.7 ± 0.1	33 ± 2	51 ± 5	120 ± 40	36 ± 12
	18	3.0 ± 0.1	36 ± 3	1.5 ± 0.1	30 ± 1	64 ± 2	174 ± 65	48 ± 20
	35	2.9 ± 0.1	37 ± 2	1.5 ± 0.1	31 ± 1	65 ± 3	87 ± 11	23 ± 3
	114	3.0 ± 0.1	37 ± 1	1.4 ± 0.1	23 ± 1	80 ± 2	97 ± 11	26 ± 3
3.0 wt % PEO-PBO	2	2.8 ± 0.1	35 ± 4	1.5 ± 0.2	24 ± 3	54 ± 4	201 ± 46	45 ± 12
	7	2.9 ± 0.1	38 ± 4	1.5 ± 0.2	30 ± 3	69 ± 5	154 ± 50	41 ± 14
	114	2.9 ± 0.1	36 ± 2	1.5 ± 0.1	24	100	101 ± 60	23 ± 13
4.7 wt % PEO-PBO	2	2.8 ± 0.1	34 ± 4	1.5 ± 0.2	24 ± 4	76 ± 6	159 ± 45	34 ± 12
	7	2.9 ± 0.1	36 ± 2	1.5 ± 0.1	29 ± 1	93 ± 4	146 ± 49	36 ± 13
	116	2.9 ± 0.1	35 ± 1	1.4 ± 0.1	24 ± 1	171 ± 1	174 ± 74	37 ± 17
6.0 wt % PEO-PBO	2	2.7 ± 0.1	28 ± 2	1.2 ± 0.1	22 ± 2	140 ± 5	148 ± 58	26 ± 13
	7	2.7 ± 0.1	30 ± 2	1.3 ± 0.1	24	165	114 ± 55	23 ± 13
	116	2.7 ± 0.1	29 ± 2	1.3 ± 0.1	20 ± 1	198 ± 3	138 ± 89	22 ± 18

^a± signifies one standard deviation about the mean based on five replicates for each sample. ^bNot every sample examined passed through the necking transition. See the Supporting Information for stress–strain data of all examined samples of 3wt % PEO-PBO aged for 114 days and 6.0 wt % PEO-PBO aged for 7 days and 116 days.

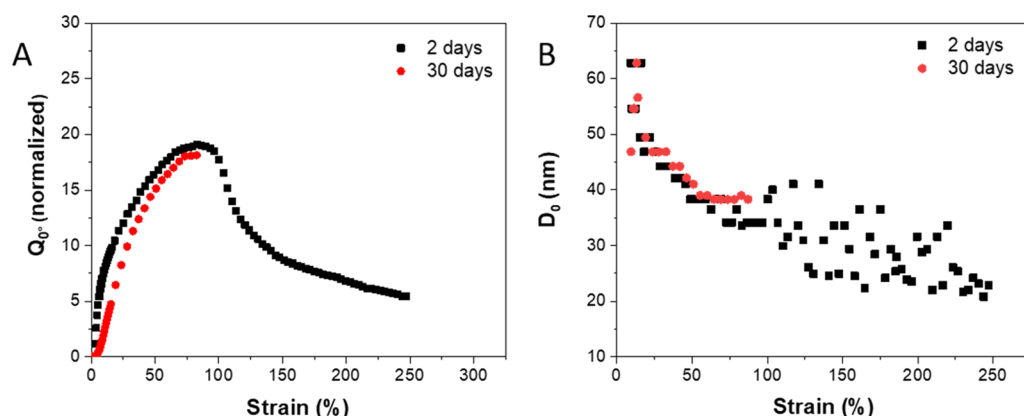


Figure 12. Plots of (A) invariant Q_0 and (B) craze fibril spacing (D_0) vs strain for 4.7 wt % PEO-PBO in PLA examined at two different aging times (i.e., 2 and 30 days).

the technological significance of this work. At short aging times (2 days), the particles can cavitate and act as stress concentrators for the development of crazes. The size of the particle dictates the craze initiation stress, with bigger particles possessing lower craze initiation stresses. The extent of crazing and the elongation prior to which crazing was the dominant toughening mechanism (or necking transition strain) were dependent on the PEO-PBO loading in PLA. As the material is further elongated, the flow stress was eventually reached, and the material would neck and flow at the necking transition. But, at longer aging times, the flow stress increased due to densification, leading to a decrease in elongation at break. The PEO-PBO/PLA blend was able to extend to relatively large strains (close to necking transition strain) and remain tough because the craze initiation and propagation were independent of aging time. Therefore, crazing induced from cavitation of properly sized particles is an effective way to overcome physical aging-induced embrittlement of glassy polymers such as PLA.

■ ASSOCIATED CONTENT

SI Supporting Information

The Supporting Information is available free of charge at <https://pubs.acs.org/doi/10.1021/acs.macromol.0c01759>.

Synthetic details; PEO-PBO/PLA blend NMR spectrum; SEC chromatograms; particle size analysis; in situ SAXS during the tensile testing setup; tensile bar images; SEM of neat PLA and blends; DSC thermograms of neat PLA and blends; compiled tensile test data; and justification for G_{1cz} (PDF)

■ AUTHOR INFORMATION

Corresponding Authors

Frank S. Bates — Department of Chemical Engineering and Materials Science, University of Minnesota, Minneapolis, Minnesota 55455, United States; orcid.org/0000-0003-3977-1278; Email: bates001@umn.edu

Christopher J. Ellison — Department of Chemical Engineering and Materials Science, University of Minnesota, Minneapolis, Minnesota 55455, United States; orcid.org/0000-0002-0393-2941; Email: cellison@umn.edu

Authors

Charles J. McCutcheon — Department of Chemical Engineering and Materials Science, University of Minnesota, Minneapolis, Minnesota 55455, United States

Boran Zhao — Department of Chemical Engineering and Materials Science, University of Minnesota, Minneapolis, Minnesota 55455, United States

Kailong Jin — Department of Chemical Engineering and Materials Science, University of Minnesota, Minneapolis, Minnesota 55455, United States; orcid.org/0000-0001-5428-3227

Complete contact information is available at: <https://pubs.acs.org/doi/10.1021/acs.macromol.0c01759>

Author Contributions

[†]C.J.M. and B.Z. are co-first authors. The manuscript was written through contributions of all authors. All authors have given approval to the final version of the manuscript.

Notes

The authors declare no competing financial interest.

■ ACKNOWLEDGMENTS

This work was supported primarily by the farm families of Minnesota and their corn check-off investment, and in part by the National Science Foundation Center for Sustainable Polymers at the University of Minnesota, a Center for Chemical Innovation (CHE-1901635). SAXS experiments were conducted at the Advanced Photon Source (APS), Sector 5 (DuPont-Northwestern-Dow Collaborative Access Team, DND-CAT). DND-CAT is supported by E.I. DuPont de Nemours & Co., The Dow Chemical Company, and Northwestern University. Use of the APS, an Office of Science User Facility operated for the U.S. Department of Energy (DOE) Office of Science by Argonne National Laboratory, was supported by the U.S. DOE under contract no. DE-AC02-06CH11357. SAXS data were collected using an instrument funded by the National Science Foundation under grant no. 0960140. Part of this work was carried out in the Characterization Facility at the University of Minnesota, which receives partial support from the NSF through the MRSEC program (DMR-2011401).

■ REFERENCES

- (1) Geyer, R.; Jambeck, J. R.; Law, K. L. Production, use, and fate of all plastics ever made. *Sci. Adv.* **2017**, 3, No. e1700782.
- (2) Jambeck, J. R.; Geyer, R.; Wilcox, C.; Siegler, T. R.; Perryman, M.; Andrady, A.; Narayan, R.; Law, K. L. Plastic waste inputs from land into the ocean. *Science* **2015**, 347, 768.

- (3) Miller, S. A. Sustainable Polymers: Opportunities for the Next Decade. *ACS Macro Lett.* **2013**, *2*, 550–554.
- (4) Liu, H.; Zhang, J. Research progress in toughening modification of poly(lactic acid). *J. Polym. Sci., Part B: Polym. Phys.* **2011**, *49*, 1051–1083.
- (5) Jem, K. J.; Tan, B. The development and challenges of poly(lactic acid) and poly(glycolic acid). *Adv. Ind. Eng. Polym. Res.* **2020**, *3*, 60–70.
- (6) Li, T. *Realizing Enhanced Toughness in Block Copolymer Modified Brittle Plastics*. University of Minnesota, 2016.
- (7) Struik, L. C. E. Physical aging in plastics and other glassy materials. *Polym. Eng. Sci.* **1977**, *17*, 165–173.
- (8) Arnold, J. C. The effects of physical aging on the brittle fracture behavior of polymers. *Polym. Eng. Sci.* **1995**, *35*, 165–169.
- (9) Haugan, I. N.; Lee, B.; Maher, M. J.; Zografos, A.; Schibur, H. J.; Jones, S. D.; Hillmyer, M. A.; Bates, F. S. Physical Aging of Polylactide-Based Graft Block Polymers. *Macromolecules* **2019**, *52*, 8878–8894.
- (10) Pan, P.; Zhu, B.; Inoue, Y. Enthalpy Relaxation and Embrittlement of Poly(l-lactide) during Physical Aging. *Macromolecules* **2007**, *40*, 9664–9671.
- (11) Theryo, G. *Deformation and physical aging of rubber-modified polylactide graft copolymers*. University of Minnesota, 2014.
- (12) Ren, J.; Urakawa, O.; Adachi, K. Dielectric and Viscoelastic Studies of Segmental and Normal Mode Relaxations in Undiluted Poly(d,l-lactic acid). *Macromolecules* **2003**, *36*, 210–219.
- (13) Baiardo, M.; Frisoni, G.; Scandola, M.; Rimelen, M.; Lips, D.; Ruffieux, K.; Wintermantel, E. Thermal and mechanical properties of plasticized poly(L-lactic acid). *J. Appl. Polym. Sci.* **2003**, *90*, 1731–1738.
- (14) Hu, Y.; Rogunova, M.; Topolkaraev, V.; Hiltner, A.; Baer, E. Aging of poly(lactide)/poly(ethylene glycol) blends. Part 1. Poly(lactide) with low stereoregularity. *Polymer* **2003**, *44*, 5701–5710.
- (15) Sheth, M.; Ananda Kumar, R.; Davé, V.; Gross, R. A.; McCarthy, S. P. Biodegradable polymer blends of poly(lactic acid) and poly(ethylene glycol). *J. Appl. Polym. Sci.* **1997**, *66*, 1495–1505.
- (16) Ljungberg, N.; Wesslén, B. The effects of plasticizers on the dynamic mechanical and thermal properties of poly(lactic acid). *J. Appl. Polym. Sci.* **2002**, *86*, 1227–1234.
- (17) Murariu, M.; Da Silva Ferreira, A.; Alexandre, M.; Dubois, P. Polylactide (PLA) designed with desired end-use properties: 1. PLA compositions with low molecular weight ester-like plasticizers and related performances. *Polym. Adv. Technol.* **2008**, *19*, 636–646.
- (18) Jacobsen, S.; Fritz, H. G.; Degée, P.; Dubois, P.; Jérôme, R. Polylactide (PLA)—a new way of production. *Polym. Eng. Sci.* **1999**, *39*, 1311–1319.
- (19) Semba, T.; Kitagawa, K.; Ishiaku, U. S.; Hamada, H. The effect of crosslinking on the mechanical properties of polylactic acid/polycaprolactone blends. *J. Appl. Polym. Sci.* **2006**, *101*, 1816–1825.
- (20) Vilay, V.; Mariatti, M.; Ahmad, Z.; Pasomsouk, K.; Todo, M. Characterization of the mechanical and thermal properties and morphological behavior of biodegradable poly(L-lactide)/poly(ϵ -caprolactone) and poly(L-lactide)/poly(butylene succinate-co-L-lactate) polymeric blends. *J. Appl. Polym. Sci.* **2009**, *114*, 1784–1792.
- (21) Anderson, K. S.; Hillmyer, M. A. The influence of block copolymer microstructure on the toughness of compatibilized polylactide/polyethylene blends. *Polymer* **2004**, *45*, 8809–8823.
- (22) Anderson, K. S.; Lim, S. H.; Hillmyer, M. A. Toughening of polylactide by melt blending with linear low-density polyethylene. *J. Appl. Polym. Sci.* **2003**, *89*, 3757–3768.
- (23) Wang, Y.; Li, K.; Zhao, X.; Tekinalp, H.; Li, T.; Ozcan, S. Toughening by Nanodroplets: Polymer–Droplet Biocomposite with Anomalous Toughness. *Macromolecules* **2020**, *53*, 4568–4576.
- (24) Dong, W.; He, M.; Wang, H.; Ren, F.; Zhang, J.; Zhao, X.; Li, Y. PLLA/ABS Blends Compatibilized by Reactive Comb Polymers: Double T_g Depression and Significantly Improved Toughness. *ACS Sustainable Chem. Eng.* **2015**, *3*, 2542–2550.
- (25) Argon, A. S. *The Physics of Deformation and Fracture of Polymers*. Cambridge university Press: united kingdom, 2013.
- (26) Bucknall, C. B. *Toughened plastics*. Springer: 1977, DOI: 10.1007/978-94-017-5349-4.
- (27) Zhao, X.; Hu, H.; Wang, X.; Yu, X.; Zhou, W.; Peng, S. Super tough poly(lactic acid) blends: a comprehensive review. *RSC Adv.* **2020**, *10*, 13316–13368.
- (28) Bai, H.; Huang, C.; Xiu, H.; Gao, Y.; Zhang, Q.; Fu, Q. Toughening of poly(l-lactide) with poly(ϵ -caprolactone): Combined effects of matrix crystallization and impact modifier particle size. *Polymer* **2013**, *54*, 5257–5266.
- (29) Liu, H.; Song, W.; Chen, F.; Guo, L.; Zhang, J. Interaction of Microstructure and Interfacial Adhesion on Impact Performance of Polylactide (PLA) Ternary Blends. *Macromolecules* **2011**, *44*, 1513–1522.
- (30) Bates, F. S.; Fredrickson, G. H. Block Copolymers—Designer Soft Materials. *Physics Today* **1999**, *52*, 32–38.
- (31) Lai, W.-C.; Liao, W.-B.; Lin, T.-T. The effect of end groups of PEG on the crystallization behaviors of binary crystalline polymer blends PEG/PLLA. *Polymer* **2004**, *45*, 3073–3080.
- (32) Lin, J.-H.; Woo, E. M. Correlation between interactions, miscibility, and spherulite growth in crystalline/crystalline blends of poly(ethylene oxide) and polyesters. *Polymer* **2006**, *47*, 6826–6835.
- (33) Tsuji, H.; Smith, R.; Bonfield, W.; Ikada, Y. Porous biodegradable polyesters. I. Preparation of porous poly(L-lactide) films by extraction of poly(ethylene oxide) from their blends. *J. Appl. Polym. Sci.* **2000**, *75*, 629–637.
- (34) Nijenhuis, A. J.; Colstee, E.; Grijpma, D. W.; Pennings, A. J. High molecular weight poly(l-lactide) and poly(ethylene oxide) blends: thermal characterization and physical properties. *Polymer* **1996**, *37*, 5849–5857.
- (35) Younes, H.; Cohn, D. Phase separation in poly(ethylene glycol)/poly(lactic acid) blends. *Eur. Polym. J.* **1988**, *24*, 765–773.
- (36) Pluta, M.; Piorkowska, E. Tough crystalline blends of polylactide with block copolymers of ethylene glycol and propylene glycol. *Polym. Test.* **2015**, *46*, 79–87.
- (37) Kowalczyk, M.; Pluta, M.; Piorkowska, E.; Krasnikova, N. Plasticization of polylactide with block copolymers of ethylene glycol and propylene glycol. *J. Appl. Polym. Sci.* **2012**, *125*, 4292–4301.
- (38) Jia, Z.; Tan, J.; Han, C.; Yang, Y.; Dong, L. Poly(ethylene glycol-co-propylene glycol) as a macromolecular plasticizing agent for polylactide: Thermomechanical properties and aging. *J. Appl. Polym. Sci.* **2009**, *114*, 1105–1117.
- (39) Li, T.; Zhang, J.; Schneiderman, D. K.; Francis, L. F.; Bates, F. S. Toughening Glassy Poly(lactide) with Block Copolymer Micelles. *ACS Macro Lett.* **2016**, *5*, 359–364.
- (40) Gu, L.; Nessim, E. E.; Li, T.; Macosko, C. W. Toughening poly(lactic acid) with poly(ethylene oxide)-poly(propylene oxide)-poly(ethylene oxide) triblock copolymers. *Polymer* **2018**, *156*, 261–269.
- (41) Allgaier, J.; Willbold, S.; Chang, T. Synthesis of Hydrophobic Poly(alkylene oxide)s and Amphiphilic Poly(alkylene oxide) Block Copolymers. *Macromolecules* **2007**, *40*, 518–525.
- (42) Wu, J.; Thio, Y. S.; Bates, F. S. Structure and properties of PBO–PEO diblock copolymer modified epoxy. *J. Polym. Sci., Part B: Polym. Phys.* **2005**, *43*, 1950–1965.
- (43) Foudazi, R.; Zhao, B.; Gokun, P.; Manas-Zloczower, I.; Rowan, S. J.; Feke, D. L. The Effect of Shear on the Evolution of Morphology in High Internal Phase Emulsions Used as Templates for Structural and Functional Polymer Foams. *ACS Appl. Polym. Mater.* **2020**, *2*, 1579–1586.
- (44) Vilgis, T. A.; Noolandi, J. Theory of homopolymer-block copolymer blends. The search for a universal compatibilizer. *Macromolecules* **1990**, *23*, 2941–2947.
- (45) Lepers, J.-C.; Favis, B. D. Interfacial tension reduction and coalescence suppression in compatibilized polymer blends. *AIChE J.* **1999**, *45*, 887–895.
- (46) Donald, A. M. Crazing. In *The Physics of Glassy Polymers*, 2 ed.; R.N. Haward, R. J. Y., Ed. Springer Sciences: United Kingdom, 1997; pp. 295–343.

- (47) Donald, A. M. Failure Mechanisms in Polymeric Materials. In *Rubber Toughened Engineering Plastics*, Collyer, A. A., Ed.; Springer Sciences: United Kingdom, 1994; pp. 1–29.
- (48) Piorkowska, E.; Kulinski, Z.; Galeski, A.; Masirek, R. Plasticization of semicrystalline poly(l-lactide) with poly(propylene glycol). *Polymer* **2006**, *47*, 7178–7188.
- (49) Kulinski, Z.; Piorkowska, E.; Gadzinowska, K.; Stasiak, M. Plasticization of Poly(l-lactide) with Poly(propylene glycol). *Biomacromolecules* **2006**, *7*, 2128–2135.
- (50) Dompas, D.; Groeninckx, G.; Isogawa, M.; Hasegawa, T.; Kadokura, M. Toughening behaviour of rubber-modified thermoplastic polymers involving very small rubber particles: 2. Rubber cavitation behaviour in poly(vinyl chloride)/methyl methacrylate-butadiene-styrene graft copolymer blends. *Polymer* **1994**, *35*, 4750–4759.
- (51) Bucknall, C. B. *Rubber toughening*; Springer, Dordrecht: 1977.
- (52) Bucknall, C. B.; Paul, D. R. Notched impact behaviour of polymer blends: Part 2: Dependence of critical particle size on rubber particle volume fraction. *Polymer* **2013**, *54*, 320–329.
- (53) Bucknall, C. B.; Clayton, D.; Keast, W. E. Rubber-toughening of plastics. *J. Mater. Sci.* **1972**, *7*, 1443–1453.
- (54) Smallwood, H. M. Limiting Law of the Reinforcement of Rubber. *J. Appl. Phys.* **1944**, *15*, 758–766.
- (55) Bucknall, C. B.; Cote, F. F. P.; Partridge, I. K. Rubber toughening of plastics. *J. Mater. Sci.* **1986**, *21*, 301–306.
- (56) Bucknall, C. B. New criterion for craze initiation. *Polymer* **2007**, *48*, 1030–1041.
- (57) Ishai, O.; Coheno, L. J. Effect of Fillers and Voids on Compressive Yield of Epoxy Composites. *J. Compos. Mater.* **1968**, *2*, 302–315.
- (58) Bucknall, C. B.; Davies, P.; Partridge, I. K. Rubber toughening of plastics. *J. Mater. Sci.* **1986**, *21*, 307–313.
- (59) Collyer, A. *Rubber Toughened Engineering Plastics*; Springer Netherlands: 2012.
- (60) Sjoerdsma, S. D.; Boyens, J. P. H. The fracture probability of high impact polystyrene. *Polym. Eng. Sci.* **1994**, *34*, 86–92.
- (61) Brown, H. R.; Kramer, E. J. Craze microstructure from small-angle x-ray scattering (SAXS). *J. Macromol. Sci., Part B Phys.* **1981**, *19*, 487–522.
- (62) Stoclet, G.; Lefebvre, J. M.; Séguéla, R.; Vanmansart, C. In-situ SAXS study of the plastic deformation behavior of polylactide upon cold-drawing. *Polymer* **2014**, *55*, 1817–1828.
- (63) He, C.; Donald, A. M.; Butler, M. F.; Diat, O. In-situ deformation studies of rubber toughened PMMA: A SAXS analysis of the response of core-shell particles to deformation. *Macromol. Symp.* **1996**, *112*, 115–122.
- (64) Mills, P. J.; Kramer, E. J.; Brown, H. R. Real time small-angle X-ray scattering from polystyrene crazes during fatigue. *J. Mater. Sci.* **1985**, *20*, 4413–4420.
- (65) Donald, A. M.; Kramer, E. J. The mechanism for craze-tip advance in glassy polymers. *Philos. Mag. A* **1981**, *43*, 857–870.
- (66) Brown, H. R.; Mills, P. J.; Kramer, E. J. A SAXS study of a single crack and craze in plasticized polystyrene. *J. Polym. Sci., Polym. Phys. Ed.* **1985**, *23*, 1857–1867.
- (67) Salomons, G. J.; Singh, M. A.; Bardouille, T.; Foran, W. A.; Capel, M. S. Small-angle X-ray scattering analysis of craze-fibril structures. *J. Appl. Crystallogr.* **1999**, *32*, 71–81.
- (68) Bucknall, C. B.; Karpodinis, A.; Zhang, X. C. A model for particle cavitation in rubber-toughened plastics. *J. Mater. Sci.* **1994**, *29*, 3377–3383.
- (69) Donald, A. M.; Kramer, E. J. Craze microstructure and molecular entanglements in polystyrene-poly(phenylene oxide) blends. *Polymer* **1982**, *23*, 461–465.
- (70) Brown, H. R.; Sindoni, Y.; Kramer, E. J.; Mills, P. J. Diffraction studies of craze structure. *Polym. Eng. Sci.* **1984**, *24*, 825–832.
- (71) Trofimchuk, E. S.; Nikonorova, N. I.; Moskvina, M. A.; Efimov, A. V.; Khavpachev, M. A.; Volynskii, A. L. Influence of liquid media on the craze initiation in amorphous polylactide. *Polymer* **2018**, *142*, 43–47.
- (72) Focatiis, D.; Martin, C.; Parsons, A. Time and Temperature Dependence of Craze Initiation in Poly(lactic acid). In *Proceedings of the Mechanics of Time Dependent Materials Conference*; Nottingham, UK, 2011.
- (73) Williams, J. G. *Fracture mechanics of polymers*. Horwood: 1984.
- (74) Bucknall, C. B.; Paul, D. R. Notched impact behavior of polymer blends: Part 1: New model for particle size dependence. *Polymer* **2009**, *50*, 5539–5548.
- (75) Zaidi, L.; Bruzaud, S.; Bourmaud, A.; Médéric, P.; Kaci, M.; Grohens, Y. Relationship between structure and rheological, mechanical and thermal properties of polylactide/Cloisite 30B nanocomposites. *J. Appl. Polym. Sci.* **2010**, *116*, 1357–1365.
- (76) Sternstein, S. S. Inhomogeneous deformation and yielding of glasslike high polymers. *Appl. Polym. Symp.* **1968**, *7*, 175–199.
- (77) Oxborough, R. J.; Bowden, P. B. A general critical-strain criterion for crazing in amorphous glassy polymers. *Philos. Mag.* **1973**, *28*, 547–559.
- (78) Sternstein, S. S. Yield criteria for plastic deformation of glassy high polymers in general stress fields. *Polym. Prepr.* **1969**, *10*, 1117–1124.
- (79) Kausch-Blecken von Schmeling, H. H.; Williams, J. G. Polymer Fracture. In *Encyclopedia of Polymer Science and Technology*, 1978; pp. 1–65.
- (80) Miller, P.; Buckley, D. J.; Kramer, E. J. Microstructure and origin of cross-tie fibrils in crazes. *J. Mater. Sci.* **1991**, *26*, 4445–4454.
- (81) Yang, A. C.-M.; Kramer, E. J. Craze fibril structure and coalescence by low-angle electron diffraction. *J. Polym. Sci., Polym. Phys. Ed.* **1985**, *23*, 1353–1367.
- (82) Maestrini, C.; Monti, L.; Kausch, H. H. Influence of particle–craze interactions on the sub-critical fracture of core–shell HIPS. *Polymer* **1996**, *37*, 1607–1619.
- (83) Kramer, E. J. In *Microscopic and molecular fundamentals of crazing*; Springer Berlin Heidelberg: Berlin, Heidelberg, 1983; pp. 1–56.
- (84) Berger, L. L.; Buckley, D. J.; Kramer, E. J.; Brown, H. R.; Bubeck, R. A. Low-angle electron diffraction from high temperature polystyrene crazes. *J. Polym. Sci., Part B: Polym. Phys.* **1987**, *25*, 1679–1697.
- (85) Kramer, E. J.; Berger, L. L. In *Fundamental processes of craze growth and fracture*; Springer Berlin Heidelberg: Berlin, Heidelberg, 1990; pp. 1–68.
- (86) Brown, H. R.; Njoku, N. G. The effect of plasticization on craze microstructure. *J. Polym. Sci., Part B: Polym. Phys.* **1986**, *24*, 11–18.
- (87) Yang, A. C. M.; Kramer, E. J.; Kuo, C. C.; Phoenix, S. L. Crazes in diluted entanglement networks of polystyrene. *Macromolecules* **1986**, *19*, 2020–2027.
- (88) Zhang, K.; Nagarajan, V.; Misra, M.; Mohanty, A. K. Supertoughened Renewable PLA Reactive Multiphase Blends System: Phase Morphology and Performance. *ACS Appl. Mater. Interfaces* **2014**, *6*, 12436–12448.
- (89) Hao, Y.; Liang, H.; Bian, J.; Sun, S.; Zhang, H.; Dong, L. Toughening of polylactide with epoxy-functionalized methyl methacrylate–butadiene copolymer. *Polym. Int.* **2014**, *63*, 660–666.
- (90) Zhang, H.; Liu, N.; Ran, X.; Han, C.; Han, L.; Zhuang, Y.; Dong, L. Toughening of polylactide by melt blending with methyl methacrylate–butadiene–styrene copolymer. *J. Appl. Polym. Sci.* **2012**, *125*, E550–E561.
- (91) Cho, K.; Yang, J.; Park, C. E. The effect of rubber particle size on toughening behaviour of rubber-modified poly(methyl methacrylate) with different test methods. *Polymer* **1998**, *39*, 3073–3081.
- (92) Hill, A. J.; Heater, K. J.; Agrawal, C. M. The effects of physical aging in polycarbonate. *J. Polym. Sci., Part B* **1990**, *28*, 387–405.
- (93) Ruokolainen, J.; Fredrickson, G. H.; Kramer, E. J.; Ryu, C. Y.; Hahn, S. F.; Magonov, S. N. Effect of Thermal History and Microdomain Orientation on Deformation and Fracture Properties of Poly(cyclohexylethylene)–Polyethylene Triblock Copolymers Containing Cylindrical PE Domains. *Macromolecules* **2002**, *35*, 9391–9402.

- (94) Robertson, C. G.; Monat, J. E.; Wilkes, G. L. Physical aging of an amorphous polyimide: Enthalpy relaxation and mechanical property changes. *J. Polym. Sci., Part B: Polym. Phys.* **1999**, *37*, 1931–1946.
- (95) Hutchinson, J. M.; Smith, S.; Horne, B.; Gourlay, G. M. Physical Aging of Polycarbonate: Enthalpy Relaxation, Creep Response, and Yielding Behavior. *Macromolecules* **1999**, *32*, 5046–5061.
- (96) Brady, J. M. The effect of thermal ageing on impact-modified engineering resins. *Polymer* **1992**, *33*, 2981–2988.
- (97) Liu, Q.; Zhang, H.; Zhu, M.; Dong, Z.; Wu, C.; Jiang, J.; Li, X.; Luo, F.; Gao, Y.; Deng, B.; Zhang, Y.; Xing, J.; Wang, H.; Li, X. Blends of polylactide/thermoplastic elastomer: Miscibility, physical aging and crystallization behaviors. *Fibers and Polymers* **2013**, *14*, 1688–1698.
- (98) Dobircau, L.; Delpouve, N.; Herbinet, R.; Domenek, S.; Le Pluart, L.; Delbreilh, L.; Ducruet, V.; Dargent, E. Molecular mobility and physical ageing of plasticized poly(lactide). *Polym. Eng. Sci.* **2015**, *55*, 858–865.
- (99) Zubrowska, A.; Piorkowska, E.; Kowalewska, A.; Cichorek, M. Novel blends of polylactide with ethylene glycol derivatives of POSS. *Colloid Polym. Sci.* **2015**, *293*, 23–33.
- (100) Hutchinson, J. M. Physical aging of polymers. *Prog. Polym. Sci.* **1995**, *20*, 703–760.
- (101) Hodge, I. M. Enthalpy relaxation and recovery in amorphous materials. *J. Non-Cryst. Solids* **1994**, *169*, 211–266.
- (102) van Melick, H. G. H.; Govaert, L. E.; Raas, B.; Nauta, W. J.; Meijer, H. E. H. Kinetics of ageing and re-embrittlement of mechanically rejuvenated polystyrene. *Polymer* **2003**, *44*, 1171–1179.
- (103) Tant, M. R.; Moskala, E. J.; Jank, M. K.; Pecorini, T. J.; Hill, A. J. Craze Initiation and Failure in Glassy Poly(ethylene Terephthalate): The Effects of Physical Aging with and Without Exposure to Chemical Environments. In *Structure and Properties of Glassy Polymers*, American Chemical Society: 1999; Vol. 710, pp. 242–257, DOI: 10.1021/bk-1998-0710.ch017.
- (104) Ishikawa, M.; Narisawa, I. The effect of heat treatment on plane strain fracture of glassy polymers. *J. Mater. Sci.* **1983**, *18*, 2826–2834.
- (105) Deblieck, R. A. C.; van Beek, D. J. M.; Remerie, K.; Ward, I. M. Failure mechanisms in polyolefines: The role of crazing, shear yielding and the entanglement network. *Polymer* **2011**, *52*, 2979–2990.